https://doi.org/10.5194/jecats-2026-7
Preprint. Discussion started: 5 May 2026

JECATS DISCUSSIONS

Expanding spatial and temporal coverage of climate change functions: Assessment and comparison with aCCFs

Christine Frömming[1], Volker Grewe[1,2], Sigrun Matthes[1], Simone Dietmüller[1], Patrick Peter[1,2], Katrin Dahlmann[1], and Patrick Jöckel[1]

[1]Deutsches Zentrum für Luft- und Raumfahrt, Institut für Physik der Atmosphäre, Oberpfaffenhofen, Germany
[2]Delft University of Technology, Aerospace Engineering, Section Aircraft Noise and Climate Effects, Delft, the Netherlands

Correspondence: Christine Frömming (christine.froemming@dlr.de)

Abstract. Aviation contributes significantly to climate change through CO_2 emissions and non-CO_2 effects such as contrail cirrus and ozone formation. As the latter effects depend strongly on location and time of emission, non-CO_2 impacts could be mitigated through optimized routing. Climate Change Functions (CCFs) and algorithmic Climate Change Functions (aCCFs) provide spatially and temporally resolved information on the effect of aviation emissions on the atmosphere, which enable the planning of such eco-efficient flight routes. While CCFs are computationally demanding, aCCFs offer simplified but faster estimates based on correlations with meteorological data, facilitating climate-optimized flight planning applications. As the current applicability of aCCFs is limited to specific regions and seasons according to previously available CCF calculations, this study aims to address these limitations by expanding the spatial and temporal scope of CCFs and by comparing results with existing aCCFs beyond their original temporal and spatial domain. Dedicated contrail and chemistry simulations were accomplished by means of a Lagrangian approach within the ECHAM/MESSy Atmospheric Chemistry (EMAC) climate model to calculate CCFs for a new date and new regions. This study advances aviation non-CO_2 climate impact modelling by expanding CCFs to U.S. and European airspaces, to a novel season, enhanced spatial and temporal resolution of contrail effects, refining ozone radiative forcing estimates, and incorporating long-term climate responses over a 100-year time horizon. The new CCFs show consistent magnitudes and spatial gradients with earlier CCFs, but reveal systematic underestimation of contrail radiative forcing due to low optical depths. The comparison of CCFs of the present study with aCCFs outside their design region and season indicates that aCCFs capture general magnitudes and most gradients but underestimate their variability, particularly for contrails and NO_x-induced effects, and reveals limitations at certain altitudes and seasons. While aCCFs offer a fast alternative for trajectory planning, they simplify complex processes compared to detailed CCF simulations. The comprehensive model setup presented in this study describes a pathway how further refine aCCF formulations and how to expand datasets to improve accuracy and applicability outside their original domain. The new CCFs from this study expand spatial (EU and continental US) and seasonal coverage (spring) and provide valuable data to advance future aCCF formulations for broader applications.

https://doi.org/10.5194/jecats-2026-7
Preprint. Discussion started: 5 May 2026

JECATS DISCUSSIONS

1 Introduction

Aviation has a significant and undeniable role in global climate change and contributes about 3.5% to total anthropogenic effective radiative forcing (ERF) in 2018 (Lee et al., 2021). Thereby, aviation's contribution to climate change extends way beyond carbon dioxide (CO_2) emissions. Non-CO_2 effects, such as contrail cirrus formation and NO_x-induced ozone (O_3) production play a substantial role in the sector's overall climate effect. Studies indicate that contrail cirrus alone may exert a climate impact comparable to or even exceeding that of aviation's CO_2 emissions, particularly along heavily trafficked corridors like the North Atlantic flight region (e.g., Bock and Burkhardt, 2016; Teoh et al., 2022).

Unlike CO_2, which exerts a globally distributed and long-lived radiative effect, the non-CO_2 aviation effects are strongly dependent on the location and timing of emissions. This spatial and temporal sensitivity implies significant potential for reducing aviation's climate impact through strategic flight routing. To quantify and potentially mitigate these effects, climate change functions (CCFs) have been developed to express the atmospheric response to aviation emissions as functions of local meteorological conditions at the time and location of release (Grewe et al., 2014a; Frömming et al., 2021).

Algorithmic climate change functions (aCCFs) represent a promising development, enabling rapid estimation of aviation climate effects without the computational expense of comprehensive climate-chemistry simulations (van Manen and Grewe, 2019; Dietmüller et al., 2023; Yin et al., 2023). These aCCFs have increasingly been used in model studies and integrated into operational tools designed for contrail mitigation and eco-efficient routing (e.g. Lührs et al., 2021; Yin et al., 2023; Simorgh et al., 2024; Castino et al., 2024) and even real-world aviation has started practical application through pilot experiments such as the German project D-KULT (Demonstrator Klima- und Umweltfreundlicher Lufttransport, Climate and environmentally friendly air transport demonstrator (Matthes et al., 2026)) and the "100 flights trial" initiated by the AKKL (Arbeitskreis Klimaneutrale Luftfahrt, Climate-neutral aviation working group).

As aCCFs were originally developed for the North Atlantic region, primarily focusing on winter and summer seasons -in case of contrail aCCFs only winter -, the current applicability of aCCFs is constrained by temporal, spatial, and methodological limitations. As a result, the validity of using these functions "off-design"— that is, outside their intended geographical regions or seasonal contexts — remains uncertain and may introduce significant inaccuracies in contrail and other non-CO_2 climate impact assessments.

Against this background, the objectives of the present study are to advance the current understanding and modelling of aviation's non-CO_2 climate effects. This is pursued by the following points: extending the geographical coverage of CCFs by inclusion of both, the United States and European airspaces, calculating CCFs for a weather situation in a new season; revising the horizontal resolution of contrail CCFs, enhancing temporal coverage to better capture diurnal variation in contrail climate effects, implementing an improved methodology for O_3 radiative forcing (RF) parametrisation and including longer-term climate responses by adopting a time horizon of 100 years to the climate metric ATR (Average Temperature Response) following suggestions by Megill et al. (2024).

These newly calculated CCFs enable a critical evaluation of the performance of existing aCCFs derived from earlier datasets (REACT4C) and assess whether aCCFs can reliably be applied outside their original design domains in terms of geographic

https://doi.org/10.5194/jecats-2026-7
Preprint. Discussion started: 5 May 2026

region and season. This explores uncertainties regarding spatial and temporal limitations in non-CO_2-related mitigation strategies. This is of particular importance, as operational employment of non-CO_2 mitigation measures accelerates worldwide.

2 Climate change functions

2.1 Aviation Emissions and their effect on cloudiness, chemistry and climate

Aviation emissions consist of carbon dioxide (CO_2), water vapour (H_2O), nitrogen oxides (NO_x), sulfur oxides (SO_x), and soot. These emissions affect climate either directly as emission of greenhouse gases (CO_2 and H_2O emissions) or indirectly through emissions causing changes in greenhouse gases or clouds by chemical or physical processes. NO_x emissions from aviation modify the atmospheric ozone (O_3) and CH_4 chemistry. At cruise altitudes NO_x emissions cause a short-term production of O_3, which is a greenhouse gas and it's enhancement causes climate warming. At the same time, NO_x emissions cause a long-term reduction of methane (CH_4), which is also a greenhouse gas and it's reduction causes a cooling. A secondary effect of the CH_4 reduction is a long-term reduction of O_3, the primary mode ozone effect (PMO), which also causes a cooling. Additionally the CH_4 reduction causes a decrease in stratospheric water vapour, implying a very small negative climate effect. The net climate effect of these changes is complex and depends on several factors such as altitude, latitude, season, and weather situation. On average all direct and indirect effects caused by NO_x emissions tend to cause a climate warming (Lee et al., 2021). Another important effect caused by aviation emissions is the formation of contrails and contrail induced cloudiness. Contrails form at cruise levels through the emission of hot and moist aircraft exhaust into cold and humid air. These contrails may persist, depending on the supersaturation with respect to ice of the ambient air, and may spread and form extensive contrail cirrus. On average, contrails and contrail cirrus cause a climate warming (Lee et al., 2021), however depending on several factors such as particle shape and solar zenith angle they can also cause a cooling (Meerkötter et al., 1999; Markowicz and Witek, 2011). Within this work we do not distinguish between line-shaped contrails and contrail cirrus but generally refer to contrails. The emission of aerosols or aerosol precursors have a direct effect on climate, which can be warming (soot) or cooling (SO_x). They can also have an indirect effect on clouds, which is still uncertain (Righi et al., 2023). Nevertheless, the effect of aerosols has not been included in the present study. Overall, the direct and indirect effects from CO_2 and non-CO_2 emissions from aviation comprise about 3.5 % of the total anthropogenic climate impact (in terms of effective radiative forcing). While other sectors reduce their emissions, the aviation sector has grown over the last decade at an annual rate of 1.1 % (Lee et al., 2021). The non-CO_2 aviation effects are highly dependent on chemical and meteorological conditions at the time and location of their emission. These conditions vary with geographic region, altitude, time of day, solar radiation, and prevailing weather pattern. As a result, certain regions and times are more sensitive to these emissions. By adjusting flight trajectories to avoid high-sensitivity areas, it is in principle possible to reduce the climate impact of aviation (e.g Matthes et al., 2012; Grewe et al., 2014a; Niklaß et al., 2019; Yin et al., 2023; Sonabend-W et al., 2024; Simorgh and Soler, 2025).

https://doi.org/10.5194/jecats-2026-7
Preprint. Discussion started: 5 May 2026

2.2 Model description

The chemistry-climate model simulations in the present study were performed with the European Centre for Medium-Range Weather Forecasts – Hamburg (ECHAM) / Modular Earth Submodel System (MESSy) Atmospheric Chemistry (EMAC) model (version 2.52) (Joeckel et al., 2010, 2016). EMAC is a numerical chemistry climate model system and incorporates submodels for physical and chemical atmospheric processes from the troposphere up to the middle atmosphere. MESSy couples various submodels to the core atmospheric model ECHAM5 (Roeckner et al., 2006). The submodels comprise infrastructure, chemistry or physics related processes or diagnostics. The chemistry was calculated by the submodel MECCA (v3.2, Sander et al. (2011)). Non-methane hydrocarbon (NMHC) chemistry was employed, reproducing the main features of the tropospheric chemistry (Houweling et al., 1998). For Lagrangian transport of atmospheric tracers, the submodel ATTILA (Reithmeier and Sausen, 2002; Brinkop and Jöckel, 2019) was used. Other submodels including TREXP (used to define new tracers and point sources of tracers) (Joeckel et al., 2010) and AIRTRAC (determines the contribution of local emissions to the atmospheric composition) (Grewe et al., 2014a) were employed within the present study. The formation of contrails and contrail cirrus is parametrized following Burkhardt et al. (2008) and Burkhardt and Kärcher (2009). Contrail processing on Lagrangian trajectories is included in the submodel CONTRAIL as explained in detail in Grewe et al. (2014a). The submodel RAD (Dietmüller et al., 2016) calculates radiative transfer and allows multiple diagnostic radiative perturbation calls. Details of the submodels essential for the present study are explained elaborately in Grewe et al. (2014a). The model was applied with a spectral resolution of T42L41, corresponding to a quadratic Gaussian grid of ~2.8°× 2.8°in latitude and longitude and 41 vertical layers from the surface up to 5 hPa. To obtain a model condition close to a real date, the prognostic variables divergence, vorticity, temperature, and the logarithm of the surface pressure were "nudged" towards ERA-Interim reanalysis data (Dee et al., 2011) by Newtonian relaxation. The boundary layer and the stratosphere above ~70 hPa were not nudged, in between transition layers of intermediate strengths of nudging coefficients were applied. The sea surface temperatures and the sea-ice concentrations were used from ERA-Interim reanalysis data. After a spin-up period of three months, the 26 and 27 March 2014 were simulated, followed by 2 days for contrail simulations and 3 months for chemistry simulations. The details of these calculations will be explained in detail in the following section.

2.3 General Methodology to derive climate change functions

Planning of eco-efficient flight trajectories requires detailed knowledge on the sensitivity of the atmosphere with respect to aviation emissions. For this purpose, so-called climate change functions (CCFs) were calculated, which contain temporally and spatially resolved information on the climate effect of standardized aviation emissions. In this study, a numerical modelling approach is employed for calculating CCFs with the modular global chemistry climate model EMAC, which has successfully been used before (Grewe et al., 2014a; Frömming et al., 2021). The details of the methodology for the calculation of CCFs were described elaborately by Grewe et al. (2014a) and Frömming et al. (2021). In the present study, we focus on the fundamental principles of the methodology and improvements over previous CCF calculations.

By means of the chemistry-climate model EMAC, including i.a. the submodels ATTILA, AIRTRAC, CONTRAIL and TR-

https://doi.org/10.5194/jecats-2026-7
Preprint. Discussion started: 5 May 2026

EXP, the specific climate effect per unit emission was calculated for predefined emission locations, altitudes and times, so called time-region grid points. The time-region grid points are listed in Table 1 (right column). In total this results in 336 locations (8 longitudes × 7 latitudes × 6 pressure levels), while considering five emission times within 32 hours of the chosen episode. The emission times were chosen to theoretically enable the optimization of flights from Europe to the United States including the return flight or vice versa, and range over 32 hours from the 26 March 2014, 0 UTC to 27 March 2014, 8 UTC. Standardized emissions were released in the EMAC grid box in which the time-region grid point is located. The emissions were equally divided onto 50 air parcel trajectories which were randomly distributed within the respective EMAC grid box. The air parcel trajectories are advected using EMAC wind fields, with mixing parametrized by the submodel LGTMIX (Reithmeier and Sausen, 2002; Brinkop and Jöckel, 2019). The contributions to atmospheric changes from additional emissions were determined for each time-region, namely the contributions to ozone (O_3), methane (CH_4), primary mode ozone (PMO), water vapour (H_2O) and to contrail and contrail cirrus coverage and ice water content. Episodic simulations of three months or two days were performed for chemical perturbations and for contrails and contrail cirrus, respectively.

The evolution of chemical contributions from time-region emissions are calculated on Lagrangian air parcel trajectories by means of AIRTRAC, which applies simplified chemistry based on diagnosed production and loss terms from MECCA background chemistry proportionally. Additional NO_x emissions modify O_3 and CH_4 concentrations through reactions involving OH and HO_2, while H_2O emissions are only subject to loss processes such as precipitation. In most cases, NO_x emissions are removed within 30-40 days, while O_3 and CH_4 respond more gradually. Longer-term responses which are not covered within the simulation period of 3 months are estimated during post-processing.

In the atmosphere, contrails form as consequence of aircraft exhaust depending on critical values of ambient temperature and humidity (Schmidt-Appleman criterion, Schumann (1996)). If the air is supersaturated relative to ice they may persist and evolve into contrail cirrus. In EMAC, the formation and evolution of contrails and contrail cirrus in response to standardized emissions at time-region grid points is parametrized by means of the submodel CONTRAIL (Grewe et al., 2014a). Within this study, we do not distinguish between line-shaped contrails and contrail cirrus and refer to contrails, only. The ability of the atmosphere to form persistent contrails is calculated according to Burkhardt et al. (2008) and Burkhardt and Kärcher (2009) at each time step taking into account the Schmidt-Appleman criterion, critical humidity over ice, and the coverage of natural cirrus. The maximum fraction of a grid box that could be covered with contrails is termed potential contrail coverage. It is important to note, that the model version used in the present study suffers from a consistent cold bias of 3 to 5 K between 100 and 400 hPa. The effect of this bias on contrail formation is discussed in more detail in Peter et al. (2025). It leads to an overestimation of relative humidity over ice and accordingly an over-prediction of contrail-formation regions and contrail persistence. In this respect, the sizes of contrail covered areas must be considered being somewhat too large. The potential contrail coverage and other relevant background properties are transferred to Lagrangian air parcel trajectories. Actual contrail formation depends on emission in the respective grid cell with basic assumptions on initial contrail dimensions as given in Grewe et al. (2014a). Once formed, they evolve through processes such as spreading driven by vertical wind shear, sublimation, sedimentation of ice particles and deposition of water vapour. Each model-timestep the quantities are transferred between grid space and lagrangian space. The contrails formed and evolved from the emission pulse are characterized by their fractional

https://doi.org/10.5194/jecats-2026-7
Preprint. Discussion started: 5 May 2026

coverage and ice water mixing ratio. Further details of the parametrizations are elaborated in (Grewe et al., 2014a).

The local emission pulses at the time-region grid points result in 4-dimensional fields of perturbations of chemical trace gases and contrail coverage. The impact of these perturbations is quantified in terms of radiative forcing (RF). The instantaneous radiative forcing (RF_{inst}) at the tropopause is calculated online by means of the EMAC submodel RAD (Dietmüller et al., 2016) at each model time-step separately for a 4-dimensional perturbation field for each species and each time-region emission. In the present study we analyse the all-sky radiative imbalance at the tropopause, which includes radiative effects of aerosols and greenhouse gases of the background atmosphere and radiative and overlapping effects of and with natural clouds. Note that effective radiative forcing (ERF) is frequently used (IPCC, 2021), however, here we rely on stratosphere-adjusted RF (RF_{adj}), since the efficacies we apply later on are based on RF_{adj}. Hence, fast feedbacks via stratospheric temperature adjustments are included in the calculation of RF_{adj}, while other fast, as well as slow feedbacks are included through the use of efficacies. For all species, except for contrails, RF_{adj} at the tropopause was parametrized using a temporally and/or spatially resolved correlation between RF_{inst} and RF_{adj} (for details see Grewe et al. (2014a)). For contrails the difference between RF_{inst} and RF_{adj} is small (Marquart et al., 2003) and neglected here. The correlation between RF_{inst} and RF_{adj} for O_3 was updated in the present study (see section 2.4.3). Each temporally and geographically varying field of RF_{adj} caused by a pulse emission at a certain time-region grid point is condensed to one single normalized global annual mean RF_{adj} value, which is mapped back to the corresponding time-region grid point. From the RF_{adj} for each species and each time-region, the average temperature response (ATR) per unit emission is determined by means of the linear climate response model AirClim (Grewe and Stenke, 2008; Dahlmann et al., 2016). AirClim calculates the temporal evolution of the annual mean radiative forcing and the subsequent temperature response according to individual perturbation lifetimes. A pulse emission was assumed and the ATR was calculated according to business-as-usual development (BAU) for a time horizon of 100 years (F-ATR100), while including efficacies according to Dahlmann et al. (2025). Finally, for each time-region grid point and each species one annual global mean value of ATR per specific emission emerges which corresponds to the original emission location and emission time. These spatially and temporally resolved quantities are called climate-change functions (CCFs).

The first version of CCFs (Grewe et al., 2014a; Frömming et al., 2021) was calculated for five typical winter and three typical summer weather situations, which represent the variability in the Northern Atlantic region in winter and summer, as defined according to the classification of North Atlantic weather patterns by Irvine et al. (2013). In principle, these spatially and temporally resolved numerical estimates of climate impact in response to standardized local emissions comprise information that could be the basis for climate impact mitigation by flight trajectory optimization. However, as the calculation of CCFs demands very high computational effort and several months of simulation time, they cannot be used for operational eco-efficient flight planning. In addition, the CCFs provide information only for the dynamic situation they were calculated for. For that reason, algorithmic Climate Change Functions (aCCFs) were developed (van Manen and Grewe, 2019; Yin et al., 2023), which are based on regression analysis between the original CCFs and instantaneous meteorological variables. The response formulas estimate the climate effect of aviation emissions and contrails employing simplified algorithms onto meteorological data for a corresponding emission date. Another approach additionally included probability density functions for the accuracy of representing CCFs of O_3 in terms of probabilistic algorithmic Climate Change Functions (paCCFs) (Rao et al., 2024). Both, aCCFs

https://doi.org/10.5194/jecats-2026-7
Preprint. Discussion started: 5 May 2026

and paCCFs require only a small number of local meteorological parameters taken from e.g. numerical weather forecast models for the time of the emission and represent a simplified but fast methodology to provide a quantitative estimate of the specific climate effect per unit emission for a certain location, altitude and time without the necessity of computationally extensive chemistry–climate model simulations.

2.4 Updates and improvements over earlier CCF versions

In the following section, modifications over the previous CCF version (Grewe et al., 2014a; Frömming et al., 2021) are described. In addition the updates and improvements are summarized in Table 1.

	Representation in earlier version of CCFs (REACT4C)	Representation in updated version of CCFs (WeCare/Eco2Fly)
Model Simulation	EMAC T42L41(DLR), MESSy v2.42, free running, 8 generic weather situations for winter and summer	EMAC T42L41(DLR), MESSy v2.52, nudged simulation
Dates	Model dates: W1: 23.12.2000, W2:04.12.2000, W3:20.01.2001, W4: 30.01.2001, W5: 26.02.2001, S1: 30.06.2000, S2: 09.06.2000, S3:28.07.2000	26./27.03.2014 (nudged to ERA-interim)
Times	6 UTC, 12 UTC, 18 UTC	26.03.2014: 0 UTC, 8 UTC, 16 UTC, 27.03.2014: 0 UTC, 8 UTC
Domain	Northern Atlantic	Northern Atlantic + USA + EU
Time-region grid points for chemical variables	Latitudes: 30N, 35N, 40N, 50N, 60N, 80N Longitudes: 75W, 60W, 45W, 30W, 15W, 0W Pressure Levels: 200 hPa, 250 hPa, 300 hPa, 400 hPa	Latitudes: 25N, 35N, 45N, 55N, 65N, 75N, 85N Longitudes: 125W, 105W, 85W, 65W, 45W, 25W, 5W, 20E Pressure Levels: 150 hPa, 200 hPa, 250 hPa, 300 hPa, 350 hPa, 450 hPa
Time-region grid points for contrails	Latitudes: 30N, 35N, 40N, 50N, 60N, 80N Longitudes: 75W, 60W, 45W, 30W, 15W, 0W Pressure Levels: 200 hPa, 250 hPa, 300 hPa, 400 hPa	irregularly distributed grid-points corresponding to contrail formation regions on 2.8°x2.8°EMAC grid Pressure Levels: 150 hPa, 200 hPa, 250 hPa, 300 hPa, 350 hPa, 450 hPa
Conversion of instantaneous to adjusted O_3 RF	Mixture of idealized perturbations of NO_x or O_3 7 pressure levels	Consistent idealized perturbations of NO_x, higher vertical resolution between 350 and 150 hPa 12 pressure levels
Climate metric / Future scenario	Average temperature response 20 yrs, pulse emission	Average temperature response 100 yrs, business as usual future scenario

Table 1. Overview on updates within CCF calculations in the present study compared with earlier version CCFs.

2.4.1 Expansion of CCF domain

Earlier CCFs (Grewe et al., 2014a; Frömming et al., 2021) focused on the North Atlantic, as in that region, flight trajectories are not as constrained and dense than over the continents, which would allow re-routing of flights in principle without creating too many conflicts. In the present study, the region for which CCFs were calculated, was expanded from the North Atlantic Region to the United States and Western and Central Europe. The spatial extent of the CCF regions is shown in Figure 1. The inclusion of both continents allows the optimization of entire flights from the US to the EU including origin and destination. Intra-European or American domestic flights could be analysed as well. The calculation of new CCFs partly outside the initial

https://doi.org/10.5194/jecats-2026-7
Preprint. Discussion started: 5 May 2026

CCF and aCCF domain and time allows a comparison of CCFs and aCCFs while considering regional and seasonal differences at the same time.

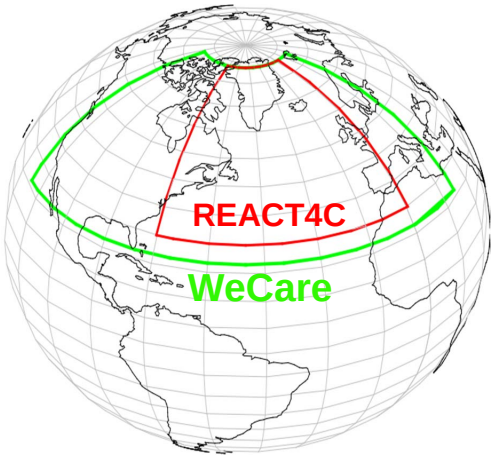

Figure 1. Region for which climate change functions (CCF) were calculated previously in REACT4C (Reducing Emissions from Aviation by Changing Trajectories for the Benefit of Climate, red), and in the present study WeCare (Utilizing Weather Information for Climate Efficient and Eco Efficient Future Aviation, green). Figure from Grewe et al. (2017)

2.4.2 Spatial resolution

The regular distribution of time-region grid points in the previous CCF version led to a latitude-longitude resolution of 5°-20°× 15°, which was, in case of contrail CCFs, too coarse to represent the distribution and small-scale structure of contrail formation areas in an adequate manner. In the present study the distribution of time-region grid points was revised for contrail simulations, so that the spatial resolution of contrail CCFs was enhanced. As a first step, the domain was masked with the actual atmospheric ability for contrail formation (potential contrail coverage) (see Figure 2). The contrail formation areas were analysed, connected areas were identified and according to the number of possible simulations, time-region grid points were distributed equally within each cohesive contrail area (Grewe et al., 2017). Concentrating on these areas ensures the avoidance of unnecessary simulations. For each irregularly distributed time-region grid point that was defined by the method above, a contrail climate response simulation was performed. The global annual mean responses resulting from the time-region grid points were interpolated within each cohesive contrail formation area. Thereby, contrail CCFs are made available on a regular grid of 2.8°× 2.8°(based on the resolution of the potential contrail coverage). With this approach the spatial resolution of contrail CCFs is increased over the earlier version of contrail CCFs, enabling the representation of considerably finer structures within the contrail CCFs without causing an increase in the number of time-region grid points nor in computation time. Despite the ability of reproducing medium scale structures with the current resolution of 2.8°× 2.8°, further refinement is certainly

https://doi.org/10.5194/jecats-2026-7
Preprint. Discussion started: 5 May 2026

necessary to resolve finer details. Note, that if aCCF formulas were derived from such CCFs, the resulting spatial resolution of calculated climate response would correspond to the resolution of the meteorological fields applied.

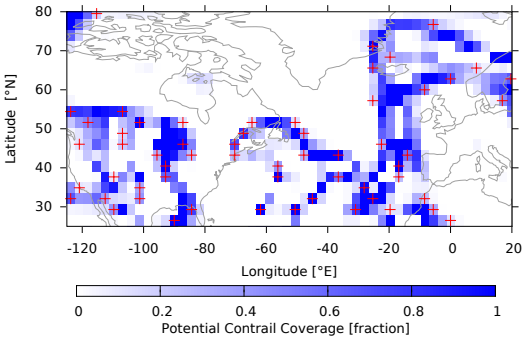

Figure 2. Irregularly distributed grid points (red crosses) used for contrail CCF calculations initialized by masking with potential contrail coverage, given as a fraction for the 26 March 2014 (blue color). Figure from Grewe et al. (2017).

2.4.3 O_3 Radiative forcing

For the evaluation of climate effects from aviation, the stratosphere-adjusted RF (RF_{adj}) is a more reliable measure than the instantaneous RF (RF_{inst}) (e.g. Hansen et al., 1997; Stuber et al., 2001). The methodology used in the present study, i.e. calculating O_3 RF from pulse emissions of NO_x does not allow the derivation of RF_{adj} directly from our simulations as this would require stratospheric temperatures to adjust to a new equilibrium. As described in detail in Grewe et al. (2014a) (Appendix), an analytical formula was devised to translate RF_{inst} from a pulse emission into an equivalent RF_{adj}. This formula was derived from a temporally and vertically resolved correlation between both RF values. Due to practical reasons, RF values from two different studies were used then, using O_3 perturbations resulting from idealized NO_x emissions (Fichter, 2009) on the one side and idealized O_3 perturbations on the other side (Stuber, 2003). The resulting correlation was coarsely resolved at typical flight altitudes. Moreover, combining the two approaches turned out to be unfavourable. An artificial minimum at 250 hPa resulted in the previous RF_{inst}/RF_{adj} fit function (Grewe et al., 2014a) (see Figure 3, dashed line) which demanded further analysis.

Within the present study, additional simulations were accomplished using a consistent and high-resolved set of O_3 perturbations resulting from idealized NO_x emissions at 12 different pressure levels from 970 hPa up to 55 hPa at northern mid-latitudes (perturbation data taken from Fichter (2009)). They determined RF_{inst} and RF_{adj} for consistent idealized O_3 perturbation pulses and allowed to revise the correlation of RF_{inst} to RF_{adj} with finer vertical resolution, as illustrated in Figure 3. The results reveal a continuous decrease of the ratio of RF_{inst} to RF_{adj} from 100 hPa with a value of almost 2 to about 0.8 at 250 hPa, while the ratio remains nearly constant below 250 hPa. The difference between RF_{inst} and RF_{adj} of a particular perturbation is generally caused by stratospheric temperature changes, which are induced by the respective perturbation (in case of RF_{adj}). O_3 perturbations which are located in the lower stratosphere cause an increase of stratospheric temperatures,

https://doi.org/10.5194/jecats-2026-7
Preprint. Discussion started: 5 May 2026

hence the ratio of RF_{adj} and RF_{inst} is above 1 for stratospheric perturbations. Whereas O_3 perturbations which are located in the troposphere cause a cooling of stratospheric temperatures, thus the ratio of RF_{adj} and RF_{inst} is below 1 for tropospheric perturbations (as shown in Figure 3). Although, the magnitude of O_3 perturbations resulting from unified NO_x emissions in the troposphere decreases with decreasing emission altitude, the distribution pattern of the perturbations over the northern extra-tropical troposphere is similar for all emission altitudes (see Fichter (2009)). This has an identical effect on both RF_{adj} and RF_{inst}, thus the ratio RF_{adj}/RF_{inst} remains constant for tropospheric emissions below 250 hPa.

As outlined by Grewe et al. (2014a) and in section 2.3 RF_{inst} is derived from the CCF simulations and is then translated into

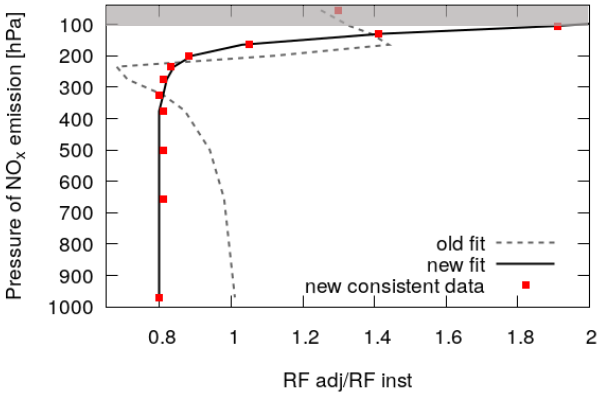

Figure 3. Ratio of stratosphere-adjusted to instantaneous O_3 RF in dependency of the emission altitude of local NO_x emissions at northern mid latitudes, where each square represents the simulation results from one O_3 perturbation pattern. O_3 perturbations from idealized NO_x emissions were taken from Fichter (2009).

equivalent RF_{adj}. While the seasonal variability of RF_{inst} and RF_{adj} is calculated as described by Grewe et al. (2014a), the altitude dependency is calculated in terms of the following (updated) fit function, which was determined using the results above and is valid for p$\geq$ 105 hPa:

$$f(p) = D + \frac{(A - D)}{(1 + \frac{p}{C}^B)} \quad (1)$$

with A=2.607, B=5.237, C=114.722, D=0.798. The CCFs calculated so far (including those of the present study) are intended for subsonic aviation and corresponding cruise levels and are valid for pressure levels between 150 hPa and 450 hPa, hence we excluded the RF_{adj} to RF_{inst} ratio above 105 hPa from the fit function, as this resulted in a better fit with minimum deviations from the data points and aCCFs are not intended for use at levels above 150 hPa anyway. Based on similar perturbation patterns (Fichter, 2009), we assume the fit being applicable both to northern and southern extra-tropics, while for tropical latitudes (30°S - 30°N) the transition from values above 1 to values smaller than 1 would shift to higher altitudes. The updated fit function for RF_{adj} was applied to the O_3-CCFs from the present study, whereas for resons of consistency O_3-CCFs from earlier studies and O_3-aCCFs remain unchanged.

https://doi.org/10.5194/jecats-2026-7
Preprint. Discussion started: 5 May 2026

2.4.4 Contrail Properties and Radiative Forcing

The formation and evolution of contrails is represented by their coverage, their ice mass and optical depth (τ). The formation of ice crystals, their advection, growth by water uptake or loss by sublimation and sedimentation, and the change in coverage by wind shear is included (Grewe et al., 2014a). The ice water content and optical depths were compared to in-situ and satellite observations and other modelling studies in Grewe et al. (2014a) and both were found to be smaller than those reported from other studies. An overview of average grid-box mean values of contrail coverage, optical depth and RF is given in Table 2. Note, that we study contrails from a single pulse emission with initial contrail widths of 200 m corresponding to a single contrail. As we determine grid-box mean values for grid box lengths of several hundred km, small quantities of coverage, τ and RF result. We identify contrail ice water contents and corresponding optical depths are considerably low in our simulations, which is not only attributed to the small contrail dimensions compared to the huge grid box sizes but also to technical reasons. These are currently revised for future versions of CCFs (Peter et al., 2026). Sporadic incorrect positive shortwave RF values occurred within our simulations, which were artificially caused by very small ice water contents and corresponding optical depths in connection with natural clouds. This matter has already been specified by Frömming et al. (2021). Contrail ages were found to be rather long compared with other studies (Gierens and Vazquez-Navarro, 2018). We found, that trajectories with long survival times exhibit particularly small coverages and optical depths. As the focus of the present study is on contrails with average lifetimes, we apply the following data sampling: We include only contrails with lifetimes up to 6 hours after formation, which is in agreement to e.g. Gierens and Vazquez-Navarro (2018); Hofer and Gierens (2025), who find mean lifetimes of 3.7 $\pm$ 2.8 h and synoptic time-scales of about 4 hours, respectively. In addition, positive shortwave RF values from contrails are excluded from the analysis (see Table 2). For future studies, the processes relevant for the termination of contrail lifetimes and for contrail properties will be revisited, for the time being the values are analysed as described.

	contrail coverage [%]	optical depth	swRF [$\mathrm{W\,m^{-2}}$]	lwRF [$\mathrm{W\,m^{-2}}$]	netRF [$\mathrm{W\,m^{-2}}$]	contrail age [h]
original	0.049	0.019	-0.00014	0.00073	0.00059	10.5
sampled	0.047	0.025	-0.00025	0.00075	0.00051	3.3

Table 2. Average grid-box mean contrail properties with and without sampling.

In general, the sign and magnitude of contrail RF depends on various influencing factors, such as the contrail optical depth, contrail altitude, particle shape, solar zenith angle and surface albedo (e.g. Meerkötter et al., 1999; Markowicz and Witek, 2011), in addition the overlap of contrails and natural clouds influences the contribution of short- and longwave to net RF (e.g. Sanz-Morere et al., 2021). Rap et al. (2010) reported a linear behaviour of contrail RF to $\tau_{contrail} \times \mathrm{b}_{contrail}$ for various combinations of contrail coverage and optical depth (for τ=0.003-0.5). Our results are at the low end compared with other modelling studies (e.g. Rap et al., 2010; Frömming et al., 2011; Burkhardt and Kärcher, 2011; Schumann et al., 2015), however, they support this linear correlation and blend in with their and other global modelling studies, if we scale our results considering

https://doi.org/10.5194/jecats-2026-7
Preprint. Discussion started: 5 May 2026

their small optical depths and dimension.

2.4.5 Climate metric

The Average Temperature Response (ATR) and the Efficacy-weighted Global Warming Potential (EGWP) were identified as most suitable climate metrics for aircraft design and aviation policy (Megill et al., 2024). For aviation policy and aircraft design, a time horizon of over 70 years is recommended by Megill et al. (2024) to reflect radiative forcing and temperature changes accurately and account for long-term climate effects. Within the present study, we follow these recommendations and choose the ATR as climate metric with a time horizon of 100 years for a business as usual future emission scenario (F-ATR100). The ATR accounts for more climate processes than the RF-based metric GWP (Global Warming Potential), while involving more assumptions and uncertainties. However, the ATR is simple to understand for non-specialists and inherently relates to temperature-based climate objectives. Grewe et al. (2014a) argued that the climate metric should reflect results from a climate-optimised scenario and suggest ATR100 for a future emission scenario (F-ATR100). In general, climate metrics differ in the ratio of CO_2 to non-CO_2 effects and conversions from one climate metric into another can be easily performed in a post-processing step (Dahlmann et al., 2025).

3 Weather situation

For our simulations of climate change functions we chose the 26 and 27 March 2014. The weather situation over Europe and the Northern Atlantic was dominated by high pressure over Scandinavia and the Azores, while low pressure was present over Central Europe with separate low pressure systems over Northern Germany and the Southern French coastal area. Frontal systems were emanating from low pressure systems over Greenland with an associated warm conveyor belt ranging from Greenland towards the eastern North Atlantic and the British Coast. The mean geopotential height and wind velocities for this period are shown in Figure 4. Ice-supersaturated regions, i.e. regions with a relative humidity over ice (rhum_{ice}) higher that 100% , with high potential contrail cirrus coverage were found over the eastern North Atlantic (Figure 4). The mean weather situation of the 26 and 27 March relative to the classification after Irvine et al. (2013) is W3 (although close to W5), which is characterized by a negative East Atlantic index and a weak jet stream which is meridionally tilted due to a high pressure ridge over the eastern North Atlantic. At this date an observation campaign took place over European mid-latitudes, ML-CIRRUS (Voigt et al. (2017)). The campaign focused on observing natural cirrus and anthropogenic contrail cirrus at mid-latitudes and investigated their microphysical and radiative properties. The selection of this date offers the possibility of a detailed comparison of model variables with observed quantities which was done by Peter et al. (2025).

https://doi.org/10.5194/jecats-2026-7
Preprint. Discussion started: 5 May 2026

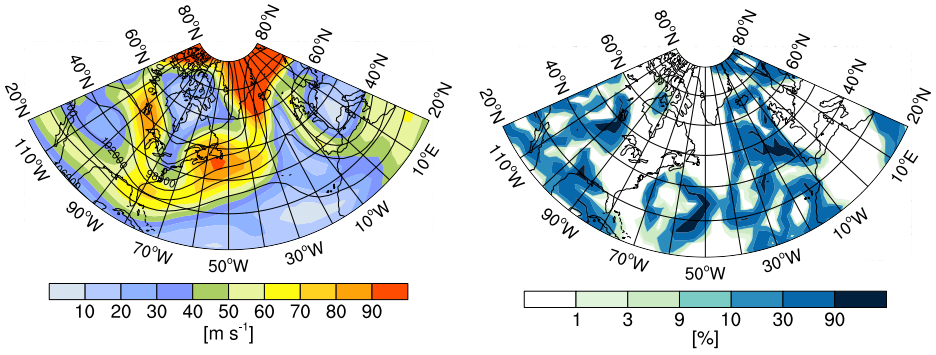

Figure 4. Mean geopotential height (black contours in gpm) and wind velocities (left) and potential contrail cirrus coverage (right) over the Northern Atlantic, Northern America and Europe at 250 hPa for 26 March 2014 as simulated with the chemistry-climate model EMAC

4 CCF Results

The Climate Change Functions determined as described in Section 2.3 are presented and analysed in the following sub-sections. The annual global mean contrail and contrail-cirrus coverage, the atmospheric contribution to O_3, CH_4 + PMO, total NO_x and H_2O and the corresponding radiative forcing and resulting average temperature response were calculated for a time horizon of 100 years for a business as usual future emission scenario (F-ATR100) from standardized emissions for every time-region grid point (see Table 1). As the individual CCFs were generated in different emission specific units, e.g. Contrail-CCFs in K/km, NO_x induced O_3- and CH_4-CCFs in K/kg(NO_2) and H_2O-CCFs in K/kg(fuel), all CCFs and aCCFs in the present study were converted to the same physical unit of K/kg(fuel) for better comparability. We used a specific range F_{km} of 0.16 km/kg(fuel) which is typical for transatlantic flights and an emission index of EI_{NOx} of 13 g(NO_2/kg(fuel)) as was done by Frömming et al. (2021) and Dietmüller et al. (2023) to receive merged CCFs and aCCFs, respectively. The global annual mean quantities of CCFs are mapped back to their original emission location and are correspondingly displayed in the maps presented in the following sections, where CCFs of all species are exemplarily shown for characteristic emission times, pressure levels and longitudes.

Histograms of CCF quantities are shown in Figure 5 for all species, all levels and emission times for 26 and 27 March 2014 as given in Table 1. The contrail-cirrus CCFs show an overall mean value of $2.9 \cdot 10^{-15}$ K/kg(fuel), being the smallest climate response, which is largely due their short lifetimes of some hours compared to weeks, months or years in case of H_2O, and NO_x induced perturbations, their small climate efficacy and comparably small optical depths (discussed in section 2.4.4). The O_3, CH_4+PMO and total NO_x CCFs show the largest absolute values, while the positive O_3 CCFs are partly compensated by the negative CH_4 CCFs of similar magnitude with mean values of $6.7 \cdot 10^{-13}$ K/kg(fuel) and -4.1 $\cdot 10^{-13}$ K/kg(fuel), respectively yielding an overall mean total NO_x effect of $1.4 \cdot 10^{-13}$ K/kg(fuel). H_2O CCFs are about one magnitude smaller than the two component effects with an overall mean value of $4.2 \cdot 10^{-14}$ K/kg(fuel), however this value is largely affected by high effects at 150 hPa, whereas at subsonic flight altitudes, H_2O CCFs are comparably smaller. If contrail-cirrus CCFs were

https://doi.org/10.5194/jecats-2026-7
Preprint. Discussion started: 5 May 2026

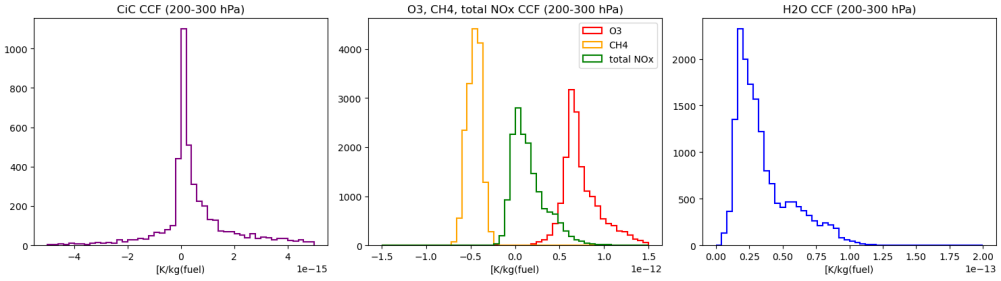

Figure 5. Distribution of CCF quantities for contrail-cirrus, total NO_x (O_3, CH_4) and H_2O in terms of F-ATR100 at 200-300 hPa for 26/27 March 2014.

scaled towards higher optical depths as those reported from other studies (e.g. Schumann et al., 2015), they may exceed other CCFs punctually. Details of the component effects are described and illustrated in the following sections.

4.1 Contrail-cirrus

Figure 6 shows the F-ATR100 for contrail-cirrus over the United States, the Northern Atlantic and Europe at pressure level 250 hPa for an emission time of 0 UTC and 8 UTC on 26 March 2014 and a zonal cross section at 15°W, exemplarily. The contrail-cirrus CCFs are inhomogeneously distributed, following the spatial structure of potential contrail-cirrus coverage (see Figure 4 for 0 UTC). The irregularly distributed time-region grid used in this study for contrail-cirrus CCFs results in a higher sampling density and therefore reveals much finer CCFs structures than earlier versions of contrail-cirrus CCFs, such as those presented by Grewe et al. (2014) and Frömming et al. (2021). Depending on local time, both positive and negative values arise. Negative values can only occur if solar radiation is present during the contrail-cirrus' lifetime, i.e. during daytime or close to sunrise and sunset, while positive values can be found at all times during day and night. At night (grey shaded) and late afternoon, contrail-cirrus have a warming climate effect as most of their lifetime occurs at night, while for an emission at 8 UTC most contrails eastwards of 30°W (not shaded) have a cooling climate effect as they occur at daytime.

Figure 7 shows the distribution of quantities for the CCF domain for all emission times on 26 and 27 March 2014. Although the values within the CCF domain are snapshots including various local times, some general statements can be made: Mostly positive contrail-cirrus CCFs are found for emission times at 0 UTC for both days as most contrail-cirrus within the domain will see no sunlight during their lifetime. Negative mean values are found for emission times at 8 UTC on both days, resulting from both positive and negative CCFs depending on individual location, local time and lifetime, while emissions at 16 UTC cause CCFs of both signs.

https://doi.org/10.5194/jecats-2026-7
Preprint. Discussion started: 5 May 2026

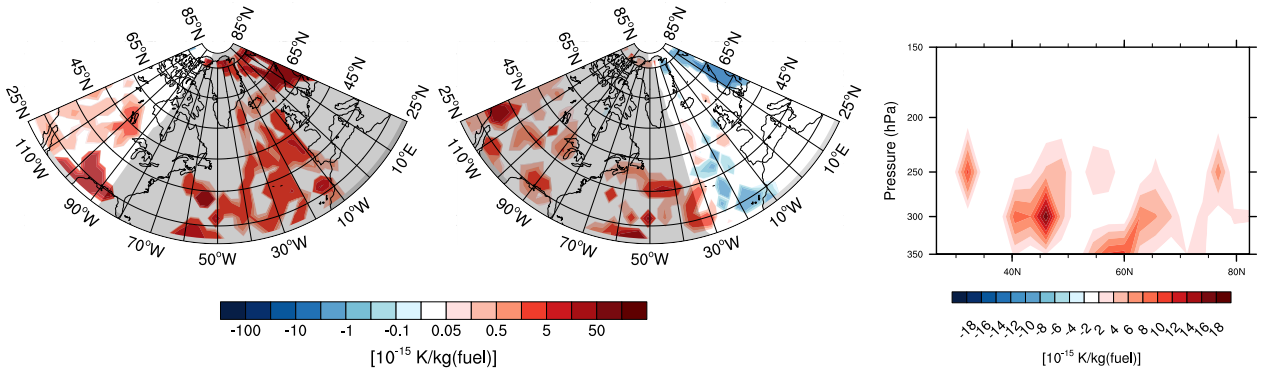

Figure 6. Contrail-cirrus CCFs on 26 March 2014 for emission times of 0 UTC (left) and 8 UTC (mid) exemplarily at 250 hPa. Grey-shaded areas indicate local night at emission time. Right: Zonal cross section of contrail-cirrus CCFs at 15°W for 26 March 2014, 0 UTC.

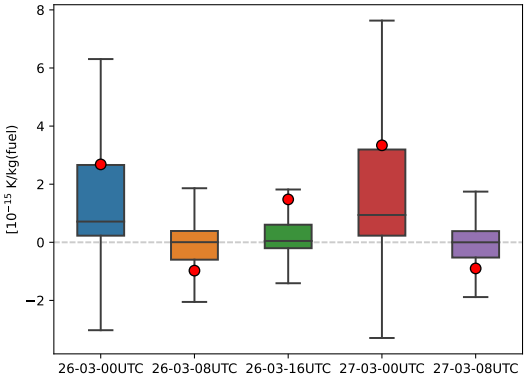

Figure 7. Boxplot of contrail-cirrus CCFs for the complete domain for different emission times on 26 and 27 March 2014, mean values are indicated by red circles. Few extreme outliers were removed.

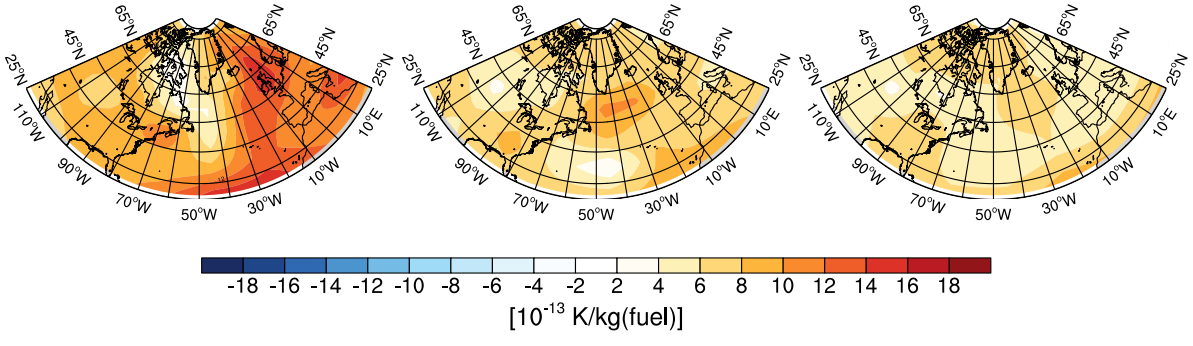

Figure 8. NO_x induced short-term O_3 CCFs for 26 March 2014 for 200 hPa (left), 250 hPa (mid) and 300 hPa (right).

https://doi.org/10.5194/jecats-2026-7
Preprint. Discussion started: 5 May 2026

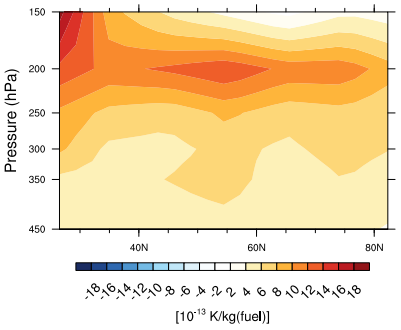

Figure 9. Zonal cross section of NO_x induced O_3 CCFs exemplarily at 15°W for 26 March 2014 (left).

4.2 Short-term Ozone

Figure 8 shows NO_x induced short-term O_3 climate change functions for the CCF domain on 26 March 2014 exemplarily for pressure levels 200 hPa to 300 hPa. O_3 CCFs are strictly positive with an overall mean of $5.0 \cdot 10^{-15}$ K/kg(fuel). Large scale circulation influences the O_3 CCF pattern resulting in higher NO_x induced O_3 responses around the high pressure ridge over the eastern North Atlantic (shown in Figure 4), while reduced values are found west of the ridge. This is in agreement with Rosanka et al. (2020) and Frömming et al. (2021) who found air masses from within high pressure ridges are transported to the tropics experiencing high ozone production efficiency while west of the ridge transport pathways are directed towards polar latitudes with minor ozone production. Figure 9 shows a zonal cross section of O_3 CCFs exemplarily at 15 °W. On average the O_3 maximum response is found at 200 hPa. At 15 °W the circulation influence with high O_3 responses is evident up to polar latitudes at 200 hPa. Above the tropopause the influence of large scale circulation declines with a domination of the latitudinal gradient and maximum values in the tropics at 150 hPa. These findings are inline with earlier climatological studies, indicating higher removal rates of aviation NO_x and reduced O_3 formation at lower flight altitudes, and enhanced photochemical O_3 production rates towards the tropics (e.g. Grewe et al., 2002; Gauss et al., 2006; Grewe and Stenke, 2008; Frömming et al., 2012). This general relationship is well reproduced by the actual version of CCFs. The altitudinal gradients were not represented as systematically in the earlier CCF version (Grewe et al., 2014a; Frömming et al., 2021) who found minimum O_3 CCFs at 250 hPa caused by the original instantaneous to adjusted RF-O_3 fit that has been revised in the present study (see sect. 2.4.3).

4.3 Methane and primary mode ozone

Figures 10 and 11 show the NO_x induced CH_4 and primary mode ozone (PMO) climate change functions over the CCF domain on 26 March 2014 for 200 hPa, 250 hPa and 300 hPa exemplarily. The climate effect of CH_4 and PMO is strictly negative with an overall mean value of -3.6 $\cdot 10^{-15}$ K/kg(fuel). Pronounced negative values of NO_x induced CH_4 and PMO CCFs are found at 200 hPa around the high pressure ridge over the eastern North Atlantic and reduced CH_4 and PMO response west of the ridge. This is in agreement with findings of Rosanka et al. (2020), who reported enhanced CH_4 depletion for emissions in high

https://doi.org/10.5194/jecats-2026-7
Preprint. Discussion started: 5 May 2026

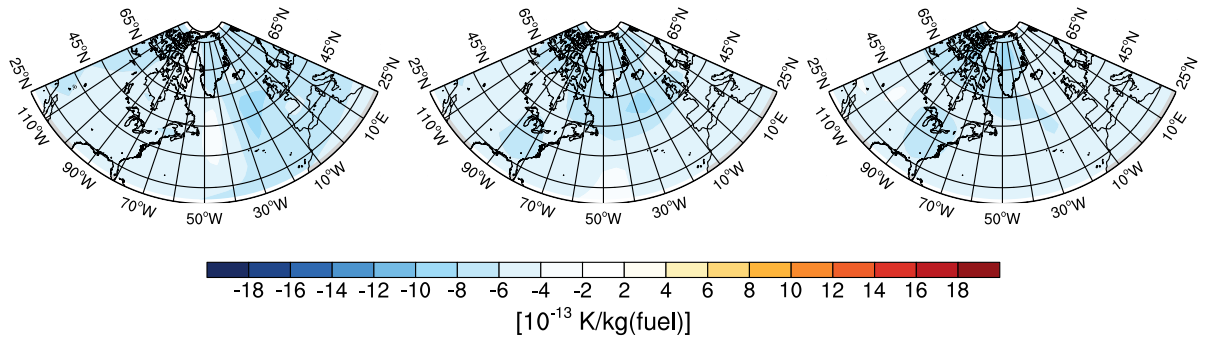

Figure 10. NO_x induced CH_4 and PMO CCFs for 26 March 2014 for 200 hPa (left), 250 hPa (mid) and 300 hPa (right).

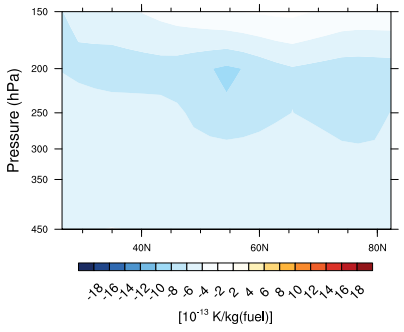

Figure 11. Zonal cross section of NO_x induced CH_4 and PMO climate change functions at 15°W for 26 March 2014.

pressure ridges, with transport towards the tropics and to lower altitudes, related to increased availability of OH precursors (H_2O and O_3). In contrast, west of the ridge (western North Atlantic), air masses remain at higher latitudes and altitudes with limited impact on methane depletion. No clear latitudinal gradient is evident in the zonal cross section (Figure 11) which is presumably caused by the specific weather situation. Only above the tropopause at 150 hPa the impact of the weather situation ceases and a latitudinal gradient emerges with NO_x induced CH_4 depletion increasing towards low latitudes. Other Studies addressing location dependent, but in contrast to our study, climatological annual mean effects of NO_x on CH_4 (e.g. Grewe and Stenke, 2008) showed an increase of the effect towards the tropics also at lower altitudes, which is potentially superimposed by circulation patterns in the present episodical study.

4.4 Total NO_x

The total NO_x effect comprises positive effects of O_3 and negative effects of CH_4 and PMO and arises from interactions between involved precursors on different spatial and temporal scales. Unlike short time horizons, which emphasize short-term effects, the choice of a time horizon of 100 years incorporates the long-term effects of aviation emissions on CH_4 and PMO ensuring a fair comparison of the time-integrated responses of all contributors to total NO_x. Figures 12 and 13 show the total

https://doi.org/10.5194/jecats-2026-7
Preprint. Discussion started: 5 May 2026

NO_x induced CCFs (O_3, CH_4 and PMO) for the CCF domain on 26 March 2014 for 200 hPa, 250 hPa and 300 hPa and a zonal cross section at 15°W, exemplarily. Depending on location, the total NO_x effect can be positive or negative. We find a positive overall mean value of $1.4 \cdot 10^{-13}$ K/kg(fuel) and a predominant positive climate effect at almost all latitudes at altitudes between 150 and 300 hPa, while a smaller negative effect can be found at altitudes up to 200 hPa at high latitudes and/or latitudes influenced by polar airmasses. Between these two areas, the sign of the total NO_x effect relies on large scale circulation, with similar dependencies than the component effects (O_3, CH_4 and PMO). Emissions experiencing transport towards the tropics tend to cause a positive total NO_x climate effect, while emissions experiencing polar influence tend to cause a negative total NO_x climate effect. At mid latitudes at 300 hPa and below, the total NO_x effect is small and rather inconclusive. The overall behaviour is in agreement with findings reported by Frömming et al. (2021). Overall, the total NO_x effect for long time horizons is rather small, due to the strong cancellation of the positive O_3 and the negative CH_4 and PMO component effects.

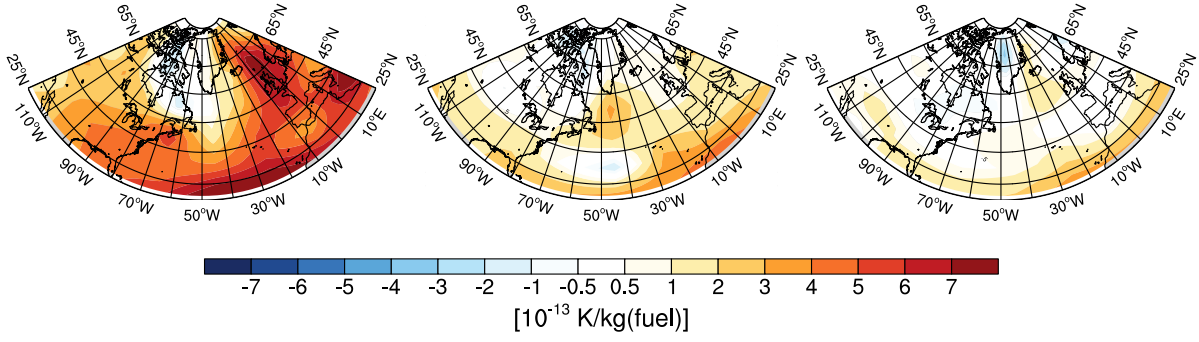

Figure 12. Total NO_x CCFs for 26 March 2014 for for 200 hPa (left), 250 hPa (mid) and 300 hPa (right).

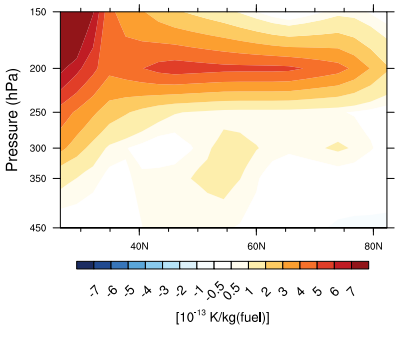

Figure 13. Zonal cross section of total NO_x climate change functions at 15°W for 26 March 2014.

https://doi.org/10.5194/jecats-2026-7
Preprint. Discussion started: 5 May 2026

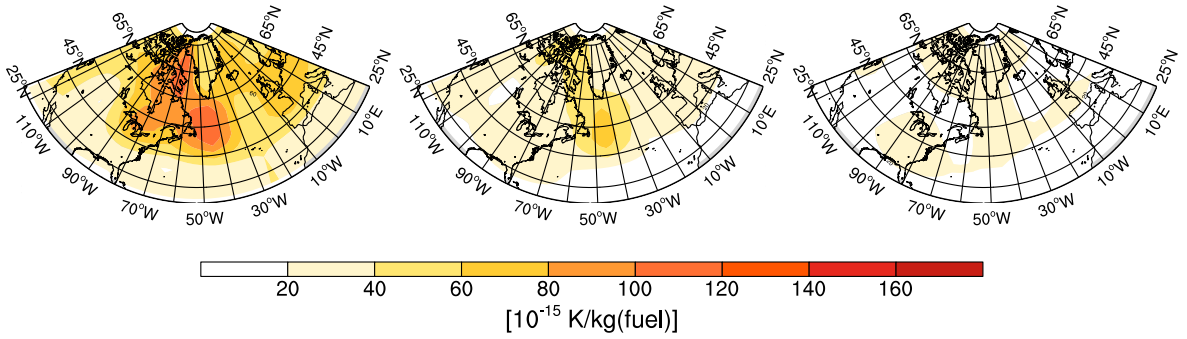

Figure 14. H_2O CCFs for 26 March 2014 for 200 hPa (left), 250 hPa (mid) and 300 hPa (right).

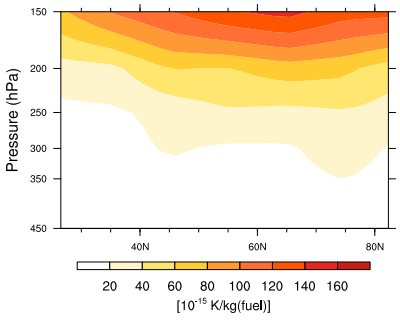

Figure 15. Zonal cross section of H_2O climate change functions at 60°W and 15°W in terms of P-ATR100 for 26 March 2014.

4.5 Water vapour

Figures 14 and 15 show H_2O CCFs for the study domain on 26 March 2014 for 200 hPa, 250 hPa and 300 hPa and a zonal cross section at 15°W, exemplarily. We find a distinct vertical gradient with a strong increase of H_2O CCFs towards high altitudes and a minor zonal gradient indicating a slight increase from the tropics towards higher latitudes. This is largely caused by an increase of loss processes and the associated reduction of perturbation lifetime towards lower altitudes and latitudes. Although H_2O CCFs are small at subsonic cruise altitudes, e.g. at 200 hPa H_2O CCFs are about one magnitude smaller than total NO_x CCFs, locally, they can have a significant impact, particularly if emissions occur in the lowermost stratosphere. In addition, H_2O CCFs could possibly gain importance for future technologies or concepts, e.g. hydrogen driven engines or higher flight altitudes as for supersonic business jets (e.g. van't Hoff et al., 2025).

5 Comparison with CCFs from REACT4C and with algorithmic Climate Change Functions

In the following section, we compare CCFs of the present study to CCFs of the REACT4C model study of winter situation W3 (Grewe et al., 2014a; Frömming et al., 2021). Weather situation W3 of REACT4C is characterized by a jet stream which is

https://doi.org/10.5194/jecats-2026-7
Preprint. Discussion started: 5 May 2026

meridionally tilted due to a high pressure ridge over the eastern North Atlantic, resembling the weather situation of 26 and 27 March 2014 of the present study. Both CCF results were derived from detailed simulations by means of the EMAC chemistry climate model but for different seasons, altitudinal and geographic domains (other differences see Table 1). Further, we compare present results to algorithmic Climate Change Functions (aCCFs) which estimate the climate effect of aviation emissions and contrails employing simplified algorithms onto meteorological data for the corresponding date. These algorithms (in case of O_3, CH_4 and H_2O) were developed on the basis of the REACT4C CCFs for 8 generic weather situations in the Northern Atlantic region for winter and summer (van Manen and Grewe, 2019; Yin et al., 2023). The algorithms for contrail-cirrus aCCFs were developed differently (Klingaman and Shine, 2023; Yin et al., 2023). Lagrangian trajectories were computed by means of a trajectory model (Methven, 1997) for ECMWF reanalysis data (Dee et al., 2011). Contrail-cirrus properties and RF were parameterized according to Schumann et al. (2012) for three winter seasons between 1994 and 2004 for the North Atlantic region between 200 and 300 hPa. The algorithms for contrail-cirrus were derived by regression analysis separately for day and night, as at night only longwave RF applies, while at day-time both short- and longwave RF is relevant (Yin et al., 2023). The AirClim model (Grewe and Stenke, 2008; Dahlmann et al., 2016) was then used for conversion from RF to ATR. Note, that for the development of aCCFs in case of O_3, CH_4 and H_2O, CCFs for winter and summer, pressure levels of 200-400 hPa, and a geographic region from 30-80°N and 0-75°W were included. While for the development of contrail-cirrus aCCFs, only data for winter, pressure levels of 200-300 hPa and a geographic region of 35-60°N and 0-75°W were included. In theory, aCCFs can be calculated for any date, altitude or region, however, so far, it is not recommended to use aCCFs outside their design space and time. In the present study, we deliberately apply aCCFs off-design in terms of season and/or region for the purpose of comparison and evaluation. The comparison of independently calculated CCFs of the present study with aCCFs based solely on meteorological input data for the corresponding date but originally derived from statistical analysis of REACT4C CCFs or CCFs based on a parametric contrail model, will give an indication to what extent the concept of simplified aCCFs is transferable to other seasons and regions outside the original development area.

5.1 Contrail-cirrus

The detailed comparison of contrail-cirrus CCFs and contrail-cirrus aCCFs revealed significant differences between the datasets. As various details and properties e.g. the optical depths of contrails underlying the contrail-cirrus aCCFs (Klingaman and Shine, 2023) were not available. We therefore reproduced the detailed calculations on which the contrail aCCF formulation is based in a slightly simplified manner (see Appendix A). In these recalculated data, we found contrail optical depths - although small compared to other studies - to be $\sim$ 2.5 times higher than those underlying the CCFs used in the present study. In addition, deviations regarding the data processing were identified. If the CCFs and aCCFs are compiled identically, we find comparable magnitudes of CCFs and aCCFs as shown in Figure 18 for 26 March 2014. The contrail climate response (given in F-ATR100) is small compared to other species due to shorter lifetime of contrails, the comparably small climate efficacy of contrails, and the general underestimation of contrail optical depths of both CCFs and aCCFs. Note that the underestimation of optical depths is addressed in present and future work (Peter et al., 2026). Figure 16 shows the geographical distribution of contrail-cirrus CCFs of REACT4C and the present study as well as contrail-cirrus aCCFs at 250 hPa. Note, that contrail CCFs of REACT4C

https://doi.org/10.5194/jecats-2026-7
Preprint. Discussion started: 5 May 2026

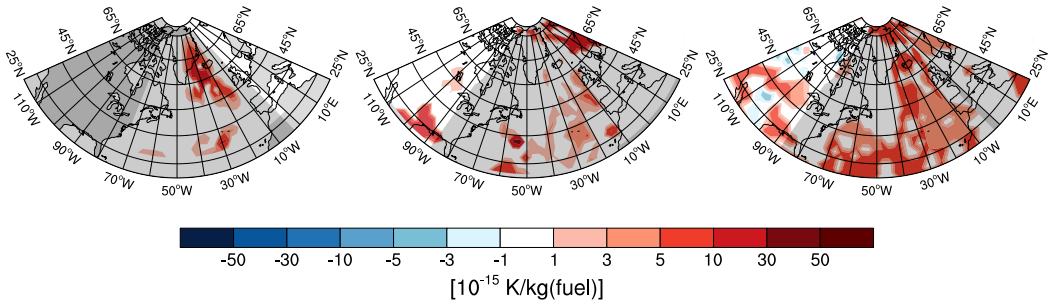

Figure 16. Contrail-cirrus CCFs from REACT4C WP2, 6 UTC (left), from the present study (mid) and aCCFs (right) for 250 hPa for 26 March 2014, 0 UTC. ACCFs are calculated using EMAC data. The grey-shaded area indicates local nighttime. Areas out of simulation domain are indicated by grey continents (only left fig.).

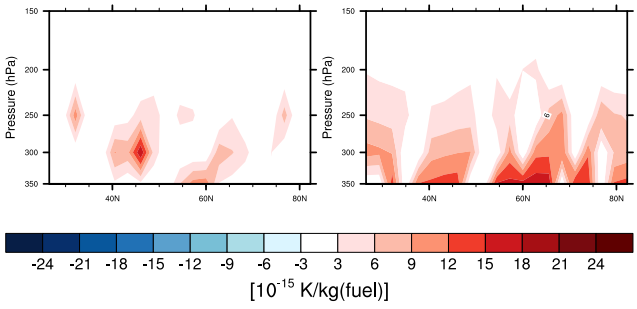

Figure 17. Comparison of zonal cross sections of Contrail-cirrus CCFs of the present study (left) and of Contrail-cirrus aCCFs (right) at 15°W, exemplarily for 26 March 2014, 0 UTC. ACCFs are calculated using EMAC data of 26 March 2014.

are shown for a different weather pattern and time (W2 at 6 UTC), therefore only the magnitude and overall structure can be compared, while the pattern deviates. The overall distribution and structure of contrail-cirrus CCFs of the present study compare reasonably well with those of aCCFs. Elongated cloud tracks along the European coast can be found in both cases as well as larger contrail covered areas over Scandinavia, the central and western North Atlantic and the Gulf of Mexico. However, over the central and south-western North American continent magnitudes and signs differ. Air traffic that produces contrails over central U.S. (local evening) partly causes cooling contrails in aCCF data, while the contrails formed in the CCF simulation lived long enough, so that a major part of their lifetime was during night, creating a warming contrail effect. Over the Atlantic some patterns coincide, however, aCCFs are spatially much more spread. The formation conditions are equal for both CCFs and aCCFs (potential contrail coverage in EMAC) at emission time and location, hence these differences can be attributed to the fact, that CCF data consider contrail properties on numerous trajectories living up to 6 hours depending on local ambient conditions, while aCCF data consider only the atmospheric conditions at time and location of emission and assume a fixed lifetime for every contrail formed. Similarly, differences in spatial distribution become obvious in the zonal cross-section in Figure 17, where contrails from CCFs at low levels dissipate according to surrounding conditions or loss processes at respective

https://doi.org/10.5194/jecats-2026-7
Preprint. Discussion started: 5 May 2026

trajectory positions, while contrails from aCCFs consider fixed conditions at formation time and location. Note, that EMAC suffers from a temperature bias, overestimating contrail formation at lower altitudes (Peter et al., 2025). A pointwise comparison and distribution of quantities of CCFs and aCCFs is shown in Figure 18. While aCCFs show a much broader, bimodal distribution with maxima on both sides of the zero line, CCFs show a narrow, unimodal distribution concentrated at very small positive values. The Pearson correlation between contrail CCFs and aCCFs is weak (r=0.2) and statistically not significant.

Although contrail-cirrus CCFs and aCCFs agree with respect to sign at nighttime (only warming), daytime values disagree

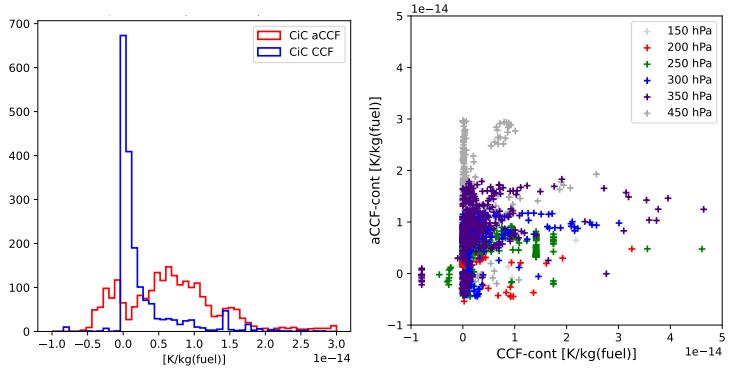

Figure 18. Histogram of contrail-cirrus CCFs and aCCFs for 26 March 2014 (0-24 UTC) (left) and pointwise comparison of contrail-cirrus CCFs and aCCFs for 26 March 2014 (0 UTC) (right). All in terms of F-ATR100. ACCFs are calculated using EMAC data.

more often in sign. CCFs indicate less cooling impact during daytime than aCCFs, which is largely caused by different methodologies and contrail assumptions. While daytime aCCFs depend on OLR only, which is a function of the temperature of the emitting body (surface, clouds) modified by atmospheric gases, daytime CCFs are controlled by various factors, such as albedo, temperature, radiative properties of contrails and natural clouds. Although the CCF calculations represent the transport of air parcels, contrail lifetimes and ambient conditions such as overlap with natural clouds more realistically, they use simplified assumptions for contrail optical properties and radiative transfer. In particular, only spherical contrail particles are assumed, while the calculations underlying aCCFs use a habit mixture of solid hexagonal columns, spatial bullet rosettes, and droxtals. Due to these differences we expect that the contrail CCFs for daytime would result in an increase of negative values if a more detailed habit mixture of contrail particles was assumed. Markowicz and Witek (2011) found the largest positive net radiative forcing for spherical particles, while hexagonal-column and hexagonal-plate particles show the smallest net radiative forcing. They found the balance between short-wave and long-wave forcing to be highly sensitive to particle shape which may even cause a change of sign of the net forcing. As the sign of contrail-CCFs is crucial for the possibility of re-routing, particle habits need to be defined more specifically in future CCF calculations.

https://doi.org/10.5194/jecats-2026-7
Preprint. Discussion started: 5 May 2026

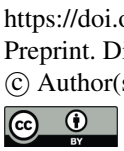

5.2 Comparison of O_3 CCFs and O_3 aCCFs

In the following, we compare O_3 CCFs of the present study to O_3 CCFs of REACT4C (W3, a comparable large-scale weather situation as the 26/27 March 2014 but in winter) and O_3 aCCFs derived by means of simplified aCCF-formulas using meteorological input data of the EMAC model for the corresponding date. Figures 19, 20, and 21 show comparative illustrations. Comparing O_3 CCFs of the present study to those of REACT4C (Fig. 19, 20 (left and mid, respectively), and Figure 21, (left), we find a similar magnitude and similar variability in both model studies, despite the different weather conditions and the different season. Similar gradients with increasing values with altitude can be identified in the zonal cross sections at 15 °W in both CCFs versions (Figure 20). The horizontal pattern (Figure 19) shows general similarities, with higher values at around 15-20 °W and lower values westwards according to large-scale circulation and higher values at low altitudes, however, the exact position and pattern of minima and maxima differs due to differences in the weather situation. Despite these differences, the overall mean deviates by less than 3%. The pointwise comparison is shown in Figure 21 showing good agreement with respect to overall magnitude and vertical distribution. A correlation coefficient of r=0.57 (Pearson) between both O_3 CCF versions is determined. If we compare O_3 CCFs of the current study with aCCFs for the same date (Fig. 19, 20, 21, left and

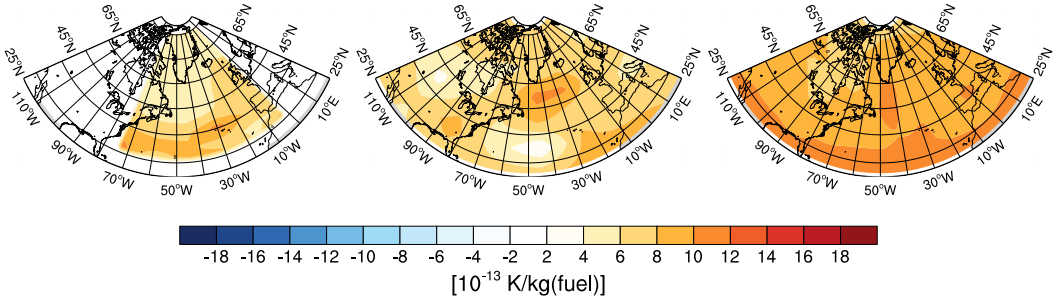

Figure 19. Comparison of O_3 CCFs of REACT4C (left), O_3 CCFs of the present study (mid) and O_3 aCCFs (right) for W3 (REACT4C) and 26 March 2014, 0 UTC, exemplarily for 250 hPa. ACCFs are calculated using EMAC data.

mid) we find aCCFs overestimating the climate effect by about 25-30% at altitudes between 200 and 300 hPa (see also van Manen and Grewe (2019)). The circulation-induced variability cannot be fully reproduced by means of the simplified aCCFs (Figure 19), however the minima, maxima and large-scale patterns roughly coincide with enhanced O_3 climate effect close to the high pressure ridge over the eastern North Atlantic and low values over North America. Between 200 and 300 hPa, the vertical gradient with increasing climate response with altitude is generally reproduced (Figure 20). Exception occurs at altitudes above 200 hPa, which were not included in the development of the algorithm (shaded in Figure 20, right), there, aCCFs continue to increase, while the CCFs decrease above 200 hPa at mid and high latitudes. A further exception occurs at altitudes below 300 hPa, where aCCFs determine an increase with decreasing altitude. This increase towards low altitudes is not supported by CCFs or other studies (e.g. Grewe and Stenke, 2008). This insufficient behaviour of aCCFs towards low altitudes was already reported by van Manen and Grewe (2019) and needs attention in future studies. The pointwise comparison (Fig.

https://doi.org/10.5194/jecats-2026-7
Preprint. Discussion started: 5 May 2026

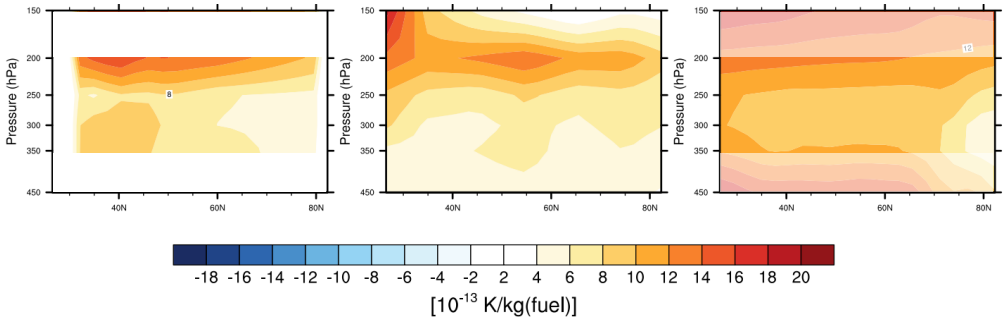

Figure 20. Comparison of zonal cross sections of O_3 CCFs of REACT4C (left) and of the present study (mid) and of O_3 aCCFs (right) at 15°W, exemplarily for W3 (REACT4C) and 26 March 2014, 0 UTC, respectively. ACCFs are calculated using EMAC data of 26 March 2014, altitudes outside the design range are shaded.

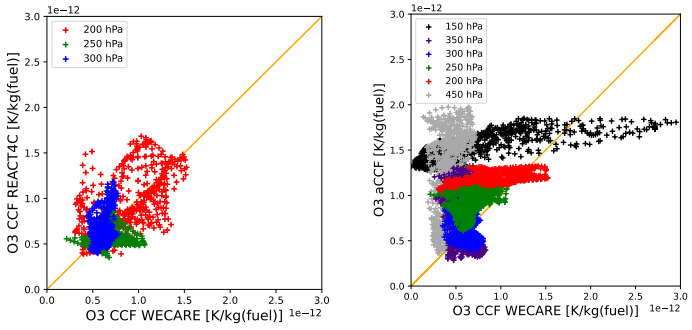

Figure 21. Pointwise comparison of O_3 CCFs of the present study versus those of REACT4C (left) and pointwise comparison of O_3 CCFs of the present study versus O_3 aCCFs. All in terms of F-ATR100 for W3 (REACT4C) and 26 March 2014, respectively. ACCFs are calculated using EMAC data. Light- and darkgrey points are vertically outside the aCCF design region.

21) reveals reduced variability of aCCFs particularly at 200 and 150 hPa. CCF simulations consider atmospheric and chemical processes for three months after emission while ACCFs consider only the situation at emission time, which is obviously not sufficient to reproduce the entire variability of the climate response. If off-design altitudes and additionally low altitudes were excluded, a correlation coefficient of r=0.48 (200-350 hPa) and r=0.57 (200-300 hPa) was found, while including all altitudes (450-150 hPa), which is not recommended, yields a deviation of overall mean values by 60% and a correlation close to random with r=0.2.

5.3 CH_4 and PMO

The following section compares CH_4 and PMO CCFs of the present study to CCFs of REACT4C and to aCCFs. Comparative visualizations are provided in Fig. 22, 23 and 24. In the present study, enhanced CH_4 loss is found for emissions around

https://doi.org/10.5194/jecats-2026-7
Preprint. Discussion started: 5 May 2026

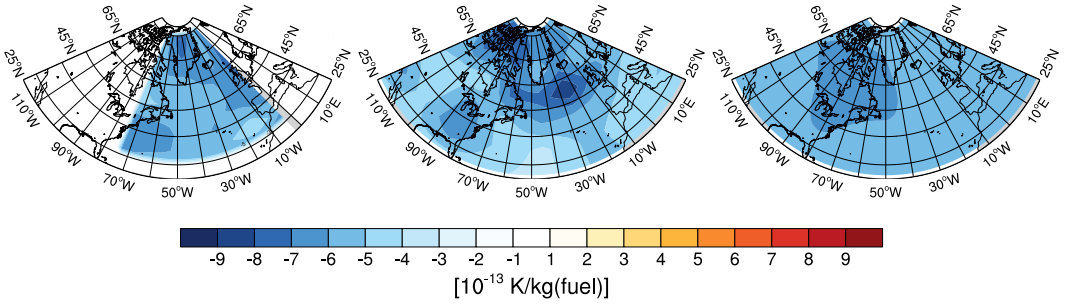

Figure 22. Comparison of CH_4 and PMO CCFs of REACT4C (left) and of the present study (mid) and CH_4 and PMO aCCFs (right) for W3 (REACT4C) and 26 March 2014, 0 UTC, respectively for 250 hPa in terms of F-ATR100. ACCFs are calculated using EMAC data.

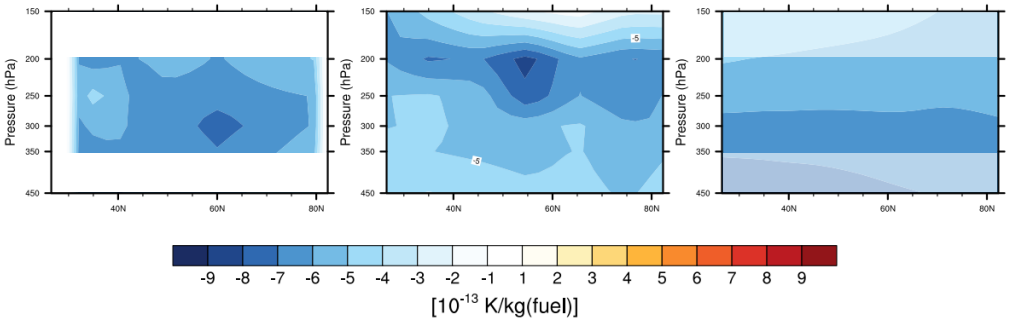

Figure 23. Comparison of zonal cross sections of CH_4 and PMO CCFs of REACT4C (left) and of the present study (mid) and CH_4 and PMO aCCFs (right) at 15°W in terms of F-ATR100 for W3 (REACT4C) and 26 March 2014, 0 UTC, respectively. ACCFs are calculated using EMAC data.

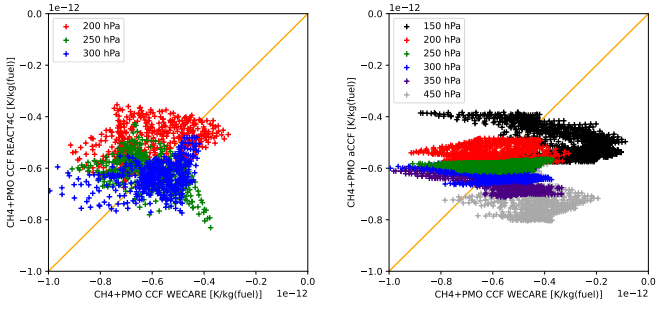

Figure 24. Pointwise comparison of CH_4+PMO CCFs of the present study versus those of REACT4C (left) and pointwise comparison of CH_4+PMO CCFs of the present study versus aCCFs. All in terms of F-ATR100 for W3 (REACT4C) and 26 March 2014, respectively. ACCFs are calculated using EMAC data. Light- and darkgrey points are outside the vertical aCCF design region.

https://doi.org/10.5194/jecats-2026-7
Preprint. Discussion started: 5 May 2026

the high pressure ridge, where emissions are transported towards the tropics, however, this relation is not very distinct in the REACT4C CCFs at 250 hPa and is not found in the aCCFs. The CCFs of the present study show a vertical gradient with maximum values around 200 hPa and a decrease towards higher and lower altitudes. There is no significant vertical gradient in the REACT4C CCFS, and there is only a minor vertical gradient in the aCCFs, which is even inverse to the gradient of the CCFs of the present study. Overall, the CH_4 and PMO aCCFs only reproduce the general magnitude but are not able to reproduce the latitudinal and circulation induced variations properly. Figure 24 shows that the variability of CH_4 and PMO is strongly underestimated by the aCCFs. Applying the CH_4 aCCFs outside the design region and season is not suggested due to this poor agreement. The correlation of the original CH_4 and PMO aCCFs was already low (r=0.17), which van Manen and Grewe (2019) identified to be unlikely to produce results accurate enough for application. Revison of CH_4 and PMO aCCFs to better capture climate response gradients should be addressed in future studies.

5.4 Total NO_x CCFs and aCCFs

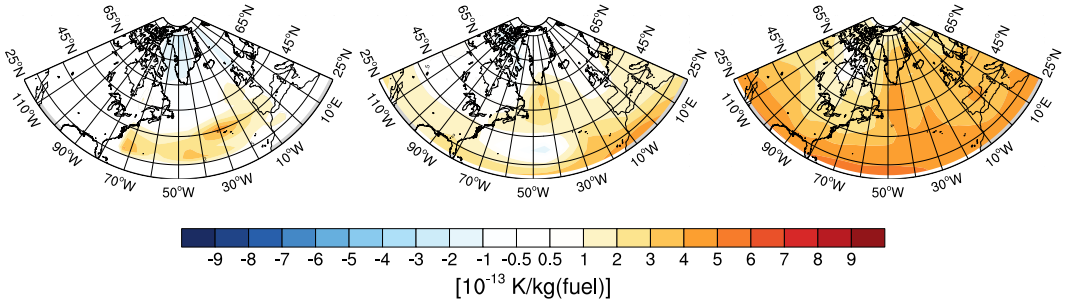

Figure 25. Comparison of total NO_x CCFs of REACT4C (left), of the present study (mid) and total NO_x aCCFs (right) for W3 (REACT4C) and 26 March 2014, 0 UTC, respectively at 250 hPa in terms of F-ATR100. ACCFs are calculated using EMAC data.

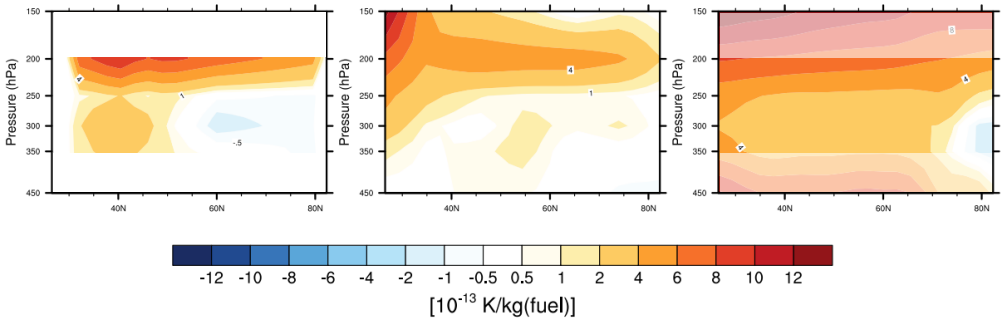

Figure 26. Comparison of zonal cross sections of total NO_x CCFs of REACT4C (left), of the present study (mid) and total NO_x aCCFs (right) at 15°W in terms of F-ATR100 for W3 (REACT4C) and 26 March 2014, 0 UTC, respectively. ACCFs are calculated using EMAC data.

https://doi.org/10.5194/jecats-2026-7
Preprint. Discussion started: 5 May 2026

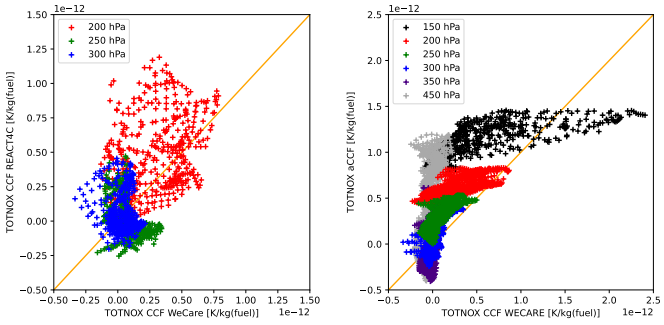

Figure 27. Pointwise comparison of total NO_x CCFs of the present study to those of REACT4C (left) and to total NO_x aCCFs (right). All in terms of F-ATR100 for W3 (REACT4C) and 26 March 2014 (CCFs present study and aCCFs), respectively. ACCFs are calculated using EMAC data. Light- and darkgrey points are outside the vertical aCCF design region.

The following section compares total NO_x CCFs and aCCFs, being illustrated by Fig. 25, 26 and 27. There is general agreement between the two versions of total NO_x CCFs (REACT4C and WECARE) in terms of large-scale structure up to 200 hPa (see Figure 25, with a predominant positive climate effect from O_3 in the tropics and subtropics and a neutral or small negative climate effect from CH_4 and PMO at high latitudes (Fig. 25 and 26. In mid-latitudes at 250 hPa a positive climate effect is found where airmasses experience tropical influence (high pressure ridge, Figure 26), whereas air masses with polar influence show a neutral or small negative climate effect (Greenland, US East coast, Figure 25). The transition from positive to negative impact fluctuates between the CCF versions depending on large-scale circulation, however, both versions compare in general with the climatological relationship between O_3 and CH_4 as analysed by Grewe and Stenke (2008) and van Manen and Grewe (2019). The aCCFs generally overestimate the total NO_x response, which is caused by the overestimation of O_3 by ~25-30%. The general large-scale pattern (minimum at US East Cost, maximum at high pressure ridge) is qualitatively similar to that of total NO_x CCFs, although shifted towards positive values. The vertical and horizontal gradient between total NO_x CCFs and aCCFs is qualitatively comparable between 200 and 300 hPa, with an increase with altitude and towards the tropics, whereas below and above aCCFs increase, while CCFs decrease (see 150 hPa and 450 hPa in Fig. 26 and 27). While the CH_4 and PMO components exhibit no significant correlation, total NO_x CCFs and aCCFs show significant positive correlations of r=0.75 (200-300 hPa), r=0.73 (200-350 hPa), and r=0.58 (150-450 hPa).

5.5 H_2O

Figure 28 compares the horizontal distribution of H_2O CCFs of the present study to those of REACT4C and to H_2O aCCFs. Figure 29 exemplarily shows zonal cross sections at 15°W for H_2O CCFs and aCCFs and Figure 30 compares H_2O CCFs of the present study to those of REACT4C and to H_2O aCCFs pointwise, for 26 March 2014 and W3 (REACT4C), respectively. H_2O CCFs from REACT4C and from the present study generally agree in terms of pattern and size despite the different seasons. H_2O climate response increases from 450 hPa to 150 hPa Figure 29 and shows high values south of Greenland and the US East

https://doi.org/10.5194/jecats-2026-7
Preprint. Discussion started: 5 May 2026

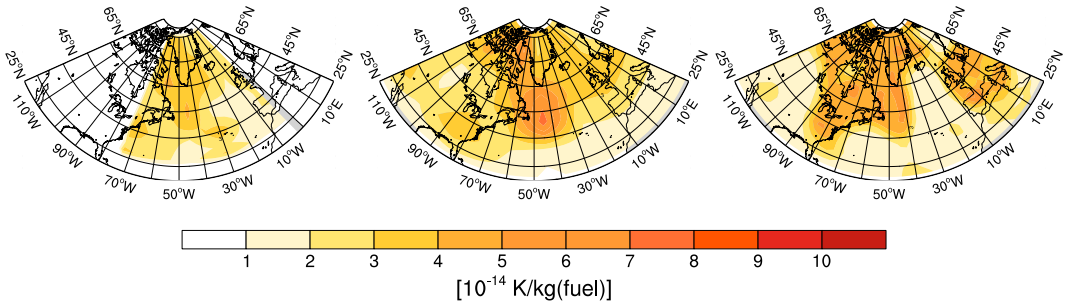

Figure 28. Comparison of H_2O CCFs of REACT4C (left), of the present study (mid) and H_2O aCCFs (right) for W3 (REACT4C) and 26 March 2014, 0 UTC, respectively, at 250 hPa in terms of F-ATR100. ACCFs are calculated using EMAC data.

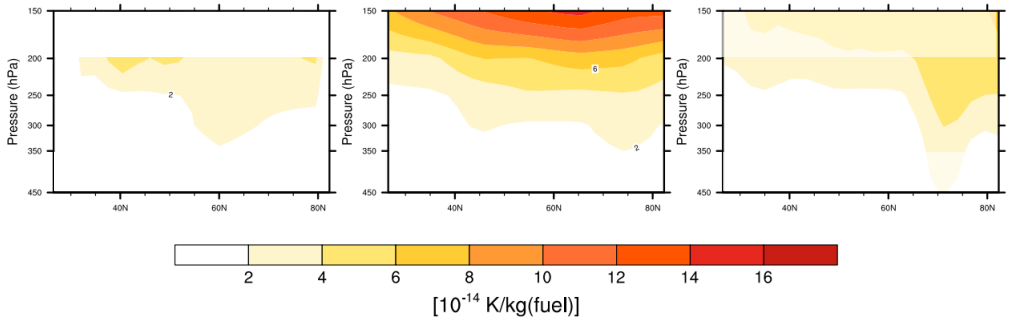

Figure 29. Comparison of zonal cross sections of H_2O CCFs of REACT4C (left), of H_2O CCFs of the present study (mid) and total NO_x aCCFs (right) at 15°W in terms of F-ATR100 for W3 (REACT4C) and 26 March 2014, 0 UTC, respectively. ACCFs are calculated using EMAC data.

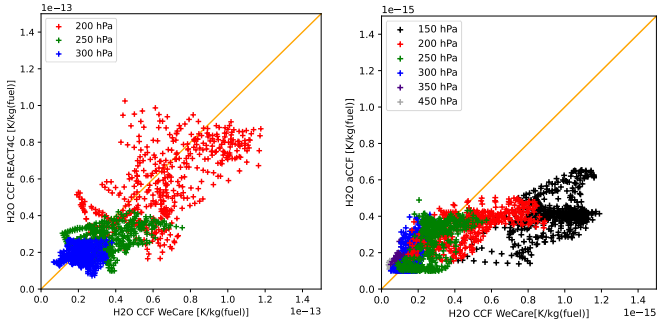

Figure 30. Pointwise comparison of H_2O CCFs of the present study to REACT4C H_2O CCFs (left) and to H_2O aCCFs (right). All in terms of F-ATR100 for W3 (REACT4C) and 26 March 2014, respectively. ACCFs are calculated using EMAC data. Light- and darkgrey points are outside the vertical aCCF design region.

https://doi.org/10.5194/jecats-2026-7
Preprint. Discussion started: 5 May 2026

Coast and low values around the high pressure ridge, which is related to low/high tropopause height. The altitudinal-, zonal- and circulation-induced variations show similar patterns in both CCF versions and are reproduced reasonably in the aCCFs at 250 and 300 hPa. However, at 200 and 150 hPa (off-design) the aCCFs underestimate the climate response by a factor of 1.5 to 2. However, the variability of CCFs is reproduced adequately (200-350 hPa) so is the relationship between background meteorology and H_2O climate effect. A comparably high correlation coefficient (Pearson) of r=0.81 is found between the two CCF versions and r=0.77 between CCFs of the present study and the aCCFs, respectively. Nevertheless, the algorithm could probably still be improved by including further seasons and additional pressure levels if a new version of aCCF formulas was developed.

6 Discussion

In the present study we introduced new Climate Change Functions (CCFs) covering an extended domain and a novel season compared to earlier versions of CCFs (Grewe et al., 2014a; Frömming et al., 2021). These new results provide the opportunity to compare the CCF versions independently to each other and to evaluate the applicability of the algorithmic Climate Change Functions (van Manen and Grewe, 2019; Yin et al., 2023) in and outside the original domain and outside the original season. In addition these new results comprise additional data to potentially advance the actual formulation of aCCFs.
We find the following major points, which we discuss in more detail in this section:

- The CCFs of the present study compare well with earlier CCFs regarding general magnitude and variability although different seasons were assessed. They show similar horizontal and vertical gradients within the shared domain.
- Contrail CCFs show systematically low optical depths. This underestimation propagates to low estimates of radiative forcing per coverage and to a systematic underestimation of contrail CCFs. The revision of optical depths in CCFs is subject of actual and future work.
- Comparing CCFs with aCCFs reveals that aCCFs successfully reproduce the overall magnitudes and most gradients within the original spatial domain despite the different season.
- Beyond the original vertical domain, gradients observed in the CCFs are not consistently represented by the current aCCF formulation in some cases.
- Identical data processing yields consistent results for contrail CCFs and aCCFs at nighttime, while at daytime higher frequency of cooling contrail aCCFs is identified, which can be attributed to differences in contrail particle properties and lifetimes.
- The O_3 aCCFs generally capture the circulation-induced horizontal gradients and vertical gradients at 200-300 hPa, yet they overestimate the climate response by 25-30% in these altitudes. The use of O_3 aCCFs outside 200-300 hPa is not recommended. Future work should incorporate data beyond the actual design region and additional seasons to mitigate this limitation.

https://doi.org/10.5194/jecats-2026-7
Preprint. Discussion started: 5 May 2026

- CH_4 and PMO aCCFs reproduce the overall magnitude of the climate response but fail to reproduce the variability in terms of horizontal and vertical gradients. There seems to be a strong weather and season dependency, which is not covered by the actual CH_4 algorithm. The actual formulation should be revisited for future applications.

- Total NO_x aCCFs qualitatively reproduce the general large-scale gradients at 200-300 hPa but overestimate the climate response by 25-30% (see O_3 aCCFs). The use of total NO_x aCCFs beyond 200-350 hPa is not recommended. Future work should incorporate data beyond the actual design region and additional seasons to mitigate this limitation.

- The H_2O aCCFs generally agree with CCFs and the underlying algorithm appears robust across seasons. Nevertheless, above 200 hPa (off-design) H_2O aCCFs underestimate the climate response by a factor of 1.5 - 2. For applications at high altitudes, the algorithm needs further development.

The overall distribution and structure of contrail CCFs and aCCFs are largely in agreement. Quantities agree if identical processing is applied to CCFs and aCCFs. However, the contrail RF underlying the CCFs is at the low end compared with other studies, which is related to systematic underestimation of contrail optical depths by about a factor of ~5 - 15. (e.g. Kärcher et al., 2010; Schumann et al., 2015). Actual and future work is addressing the underestimation of contrail optical depths in CCFs, by e.g. a lower boundary for the ice water content along the trajectories, adapting the interaction between Lagrangian emission trajectories and background trajectories and revising condensable water availability. If we compare contrail CCFs for different emission times (Figure 7), we find predominant positive net RF except at 8 UTC, while other studies (e.g. Schumann et al., 2015; Teoh et al., 2022) find higher probability of negative net RF during daytime. Incorporating a more detailed and realistic ice crystal habit mixture for contrail particles could lead to more negative (i.e., cooling) values of daytime contrail-CCFs (Markowicz and Witek, 2011), which should be considered in future CCF calculations.

Although the horizontal patterns and vertical gradients induced by general circulation agree for O_3 CCFs and aCCFs at altitudes between 200 and 300 hPa, aCCFs show reduced variability and the general magnitude is overestimated for this spring case by 25-30% (see van Manen and Grewe (2019)). If we compare the CCFs of the present study and according aCCFs for the spring date to those of all winter and summer weather situations of the REACT4C study (Figure 31), we find that the CCFs of the present study appear more like a winter situation whereas the aCCFs for the corresponding spring date lie between winter and summer. The seasonal transition from winter to spring is obviously difficult to capture adequately by the present aCCF formulation. We conclude, that the driving forces such as seasonal variability in chemical production and loss processes and physical mechanisms are not suitably described for this specific spring date. Besides, we found a strong and unrealistic increase of O_3 aCCFs at altitudes below 300 hPa and above 200 hPa that needs to be addressed in future aCCF formulas. In the meantime, O_3 and total NO_x aCCFs should not be used outside the range 200-400 hPa or even 200-300 hPa.

We compared CH_4-PMO CCFs with aCCFs and find only the general magnitude to be reproduced, whereas neither vertical nor horizontal variability or gradients are reproduced sufficiently by the aCCFs. As the CH_4+PMO effect gains relative importance for longer time horizons (as in the present study), the formulation of CH_4 aCCFs should receive further attention in future studies. Both, the CCFs and the aCCFs don't reflect the latitudinal gradient that was found in global averaged climatological studies (e.g. Grewe and Stenke, 2008). We assume a strong interference of weather related influence on the latitudinal effect of

https://doi.org/10.5194/jecats-2026-7
Preprint. Discussion started: 5 May 2026

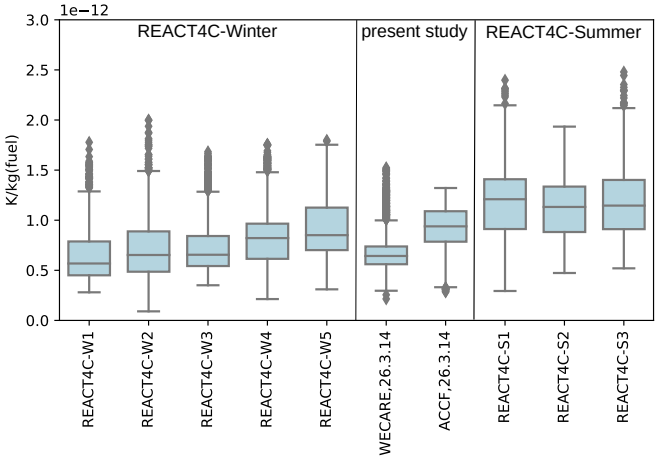

Figure 31. Boxplot showing O_3 CCFs and O_3 aCCFs for 26 March 2014 (present study) in comparison with O_3 CCFs for REACT4C winter and summer weather situations. All in terms of F-ATR100.

CH_4 at mid latitudes in the troposphere that superimposes the climatological mean effects.

The comparison of CCFs and aCCFs with respect to H_2O shows overall agreement regarding the general magnitude and vertical and horizontal gradients. The algorithm reproduces the dependencies successfully up to 250 hPa, while at 200 hPa and above (off-design) the aCCFs underestimate the climate effect systematically by a factor of 1.5 to 2. Overall, the comparison of H_2O CCFs and aCCFs seems not as affected by seasons and actual circulation differences as the other species. Nevertheless, the results suggest that the H_2O aCCFs could benefit from a vertical expansion and integrating new seasons.

In addition to the distinctions and limitations mentioned above, it is worth noting, that the aCCFs were developed from simulations for 200, 250, 300 and 400 hPa but were applied for comparison in the present study in altitudes of 150, 200, 250, 300, 350, 450 hPa. As evident from the zonal and the pointwise comparison, the CCFs and aCCFs differ considerably at 150 hPa. During the development of the algorithmic Climate Change Functions no data from this altitude were included and this region constitutes the transition to the lowermost stratosphere at mid-latitudes, where chemical and dynamical influences differ considerably to those in the troposphere. Hence, an application of the aCCF formulas above 200 hPa is not recommended. Furthermore, we recommend the application of aCCFs in winter and summer only, until the aCCFs are updated with additional data from other seasons, as planned within upcoming projects such as F4EClim (https://www.f4eclim.eu/). Outside the original development region (North Atlantic) aCCFs might be applied cautiously in the Northern Hemisphere within the original latitudes (30°N - 80°N) as these regions are controlled by similar dynamical and chemical influences.

ACCFs were deliberately developed for sort-of-instant application in theoretical or real-life climate-optimized trajectory planning to avoid time demanding chemistry climate model simulations. However, the aCCF approach could only be realized by major simplifications. ACCFs were derived by regression analysis of CCFs with local meteorological variables at the location and time of emission. The algorithms based on these regressions are used to estimate the climate effect as simple functions

https://doi.org/10.5194/jecats-2026-7
Preprint. Discussion started: 5 May 2026

of local atmospheric conditions. Not only the simplifications entail inaccuracies, but also the CCFs are subject to inherent uncertainties. Their reliability depends critically on the accuracy of the modelled atmospheric state, e.g. temperature and humidity, which are key factors for contrail formation and persistence. Systematic biases in climate models can significantly influence contrail predictions, leading to potential errors in the estimated CCFs and aCCFs (Peter et al., 2025). Nevertheless, despite the uncertainties, simplifications and limitations of aCCFs, detailed simulations by Yin et al. (2023) confirmed that climate-optimized trajectories based on NO_x induced O_3 aCCFs resulted in a reduction of O_3 climate effect compared to cost-optimized trajectories for exemplary summer and winter days.

7 Conclusions

Since aCCFs are already used by air traffic stakeholders to optimize real flight trajectories through re-routing for climate mitigation (D-KULT, AKKL), it is essential to assess their limitations. The CCFs introduced in the present study, for an extended domain and a novel season, expand our knowledge on spatially and temporally resolved aviation climate effect beyond the Northern Atlantic and across a wider altitude range. Further, these new CCFs enable a direct comparison with aCCFs. ACCFs represent a simplified relationship between meteorological quantities at the time of emission and the resulting aviation climate effect. Their fast computation and the avoidance of time consuming detailed climate chemistry simulations involves major simplifications. Our comparison revealed, that for most species, except CH_4, the overall magnitude as well as the general orientation of vertical and horizontal gradients agrees between the detailed chemistry-climate model simulations (CCFs) and the simplified formulas based on local meteorological variables (aCCFs). Yet, for O_3 and H_2O this agreement is limited to defined altitude ranges. O_3-aCCFs show reduced variability at some pressure levels and overestimate the climate response by 25-30% at 200-300 hPa, while H_2O-aCCFs underestimate the response at 150-200 hPa. These findings indicate that aCCFs can be used in limited geographic regions, altitude ranges and seasons.

Overall, the present study highlights the necessity of a targeted, species-specific advancement before aCCFs can be generally employed in mitigation scenarios and climate policy throughout the year, for all species and a wider geographic domain. The CCFs presented here, together with other available data, could provide a valuable basis for an expansion of aCCFs in terms of geographic and seasonal coverage and altitude ranges. Once the developments and expansions are addressed, aCCFs could provide a more robust basis for assessments of aviation climate effects and for the development of mitigation strategies.

Code and data availability. The Modular Earth Submodel System (MESSy) is continuously further developed and applied by a consortium of institutions. The usage of MESSy and access to the source code is licenced to all affiliates of institutions which are members of the MESSy Consortium. Institutions can become a member of the MESSy Consortium by signing the MESSy Memorandum of Understanding. More information can be found on the MESSy Consortium Website at http://www.messy-interface.org. The code presented here was based on MESSy version d2.52 and can be made available upon request. The EMAC simulation output data that were produced and analysed in this paper can be made available upon request.

https://doi.org/10.5194/jecats-2026-7
Preprint. Discussion started: 5 May 2026

Appendix A: Recalculation of contrail aCCF underlying data

A detailed comparison of contrail-cirrus CCFs and aCCFs revealed significant differences. As essential details of the methodology, data processing and contrail properties underlying the contrail-cirrus aCCFs were not available, we reproduced these calculations in a slightly simplified way for identical spatial and temporal domains as given in Klingaman and Shine (2023). Meteorological input data for the calculation of contrail radiative forcing were taken from ERA5 reanalysis data (Hersbach et al., 2020) instead of ECMWF Interim reanalysis data (Dee et al., 2011) and ECMWF IFS (Integrated Forcasting System) data. The data were regridded to a horizontal resolution of $1° \times 1°$. Similar as in Klingaman and Shine (2023) we determined the annual global mean contrail radiative forcing for the North Atlantic (35°N - 60°N, 0°W - 70°W) for pressure levels 200 hPa, 250 hPa, 300 hPa for December, January, and February of the years 1994/95, 1995/96, 2003/04. In the present study, ice supersaturation and contrail properties were calculated for static conditions instead of following Lagrangian trajectories as in Klingaman and Shine (2023). They verified the contrail persistence by ice supersaturation through humidity and temperature criteria every six hours at the actual trajectory location, while the simplified approach here does not review persistence of ice supersaturation once met, but assumes a fixed lifetime of six hours. All other steps of the radiative forcing calculation are followed as given in Klingaman and Shine (2023). Only the sampling of day- and night-time used below differs slightly.

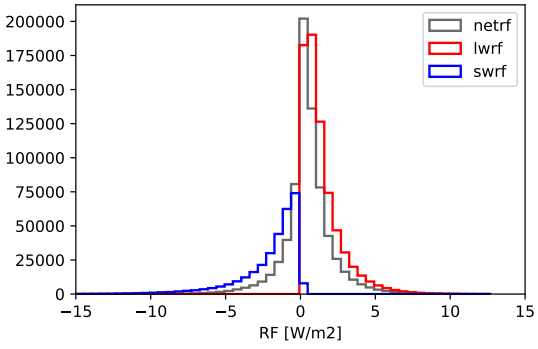

Figure A1. Histogram of local radiative forcing (shortwave, longwave, net) of recalculated contrails.

For the three winters given above, an overall mean contrail optical depth of 0.04 and an annual global mean net RF of 0.48 $\mathrm{W\,m^{-2}}$ was found. A histogram of local shortwave, longwave and netRF is presented in Fig A1. These quantities appear small compared with other studies (e.g., Schumann et al., 2015), which we found is largely caused by the assumption of a fixed vertical contrail depth of only 200 m.

Annual global mean radiative forcing comparable with Klingaman and Shine (2023) is obtained for night- and day-time contrails, as shown in Fig. A2 and A3. Extrema for both night- and day-time contrail radiative forcing reach slightly higher/lower values than in Klingaman and Shine (2023), which might be caused by different meteorological input data as well as different contrail lifetime assumptions. As shown in Fig A2, this mainly affects contrails at 300 hPa, which may experience temperature induced lifetime reductions in Klingaman and Shine (2023) due to the re-evaluation of supersaturation. Slightly different

https://doi.org/10.5194/jecats-2026-7
Preprint. Discussion started: 5 May 2026

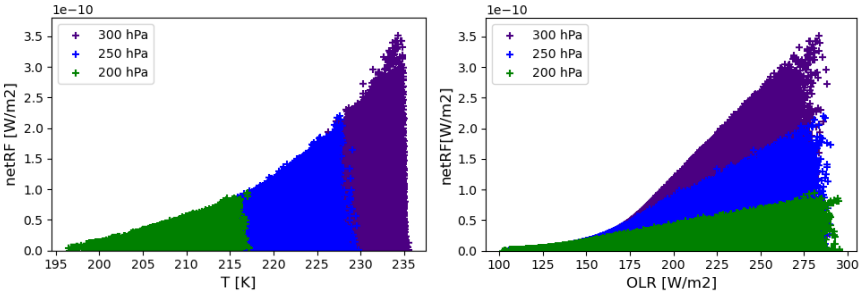

Figure A2. Scatterplots of annual global mean net radiative forcing of night-time contrails (0 UTC) versus temperature (left) and outgoing longwave radiation (OLR, right) for comparison with Klingaman and Shine (2023).

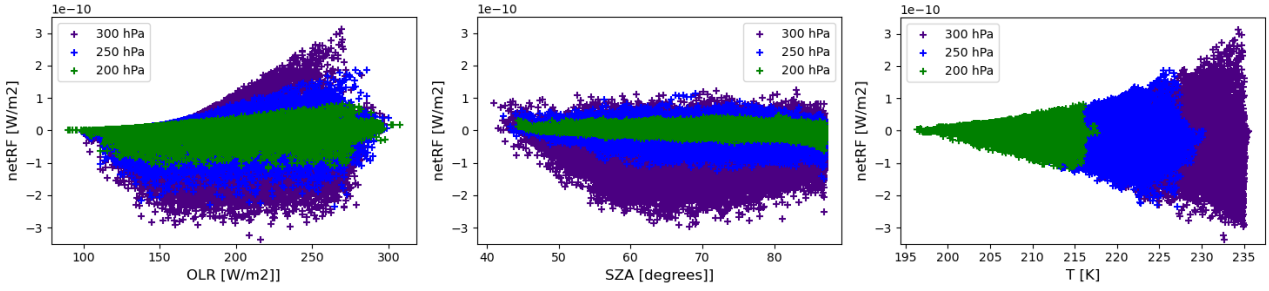

Figure A3. Scatterplots of annual global mean net radiative forcing of day-time contrails (12 UTC) versus outgoing longwave radiation (OLR, left), solar zenith angle (SZA, mid) and temperature (right) for comparison with Klingaman and Shine (2023).

correlations of contrail radiative forcing to other quantities (temperature, outgoing longwave radiation, solar zenith angle) are found, which might be caused by the simplified methodology, different lifetime assumptions and different meteorological input data, as well as slightly different temporal distinction between day/night (0 UTC/12 UTC). The simplified methodology served our purpose to relate to the general methodology and determine missing quantities such as contrail optical depths, radiative forcing and details of the data processing.

Author contributions. CF, VG and PJ developed the code. CF and VG designed the experiments. CF performed the simulations, analysed the results and wrote the manuscript. KD provided metric conversion factors. All co-authors reviewed the text and contributed to the discussion.

Competing interests. At least one of the co-authors is a member of the editorial board of JECATS.

https://doi.org/10.5194/jecats-2026-7
Preprint. Discussion started: 5 May 2026

Acknowledgements. Computational resources for calculating the CCFs were made available by the German Climate Computing Center (DKRZ) through support from the German Federal Ministry of Education and Research (BMBF). We thank Simon Kirschler (DLR) for internally reviewing a draft version of the manuscript.

Financial support. This study was supported by the DLR aviation research programme (WeCare, Eco2Fly). Further funding was obtained via the Luftfahrtforschungsprogramm (LuFo VI, D-KULT) by the Federal Ministry for Economic Affairs and Energy (formerly Federal Ministry for Economic Affairs and Climate Protection).

https://doi.org/10.5194/jecats-2026-7
Preprint. Discussion started: 5 May 2026

JECATS DISCUSSIONS

References

Bock, L. and Burkhardt, U.: Reassessing properties and radiative forcing of contrail cirrus using a climate model, Journal of Geophysical Research, 121, 9717 – 9736, 2016.

Brinkop, S. and Jöckel, P.: ATTILA 4.0: Lagrangian advective and convective transport of passive tracers within the ECHAM5/MESSy (2.53.0) chemistry-climate model, Geoscientific Model Development, 12, 1991–2008, https://doi.org/10.5194/gmd-12-1991-2019, 2019.

Burkhardt, U. and Kärcher, B.: Process-based simulation of contrail cirrus in a global climate model, Journal of Geophysical Research Atmospheres, 114, https://doi.org/10.1029/2008JD011491, 2009.

Burkhardt, U. and Kärcher, B.: Global radiative forcing from contrail cirrus, Nature Climate Change, 1, 54 – 58, https://doi.org/10.1038/nclimate1068, 2011.

Burkhardt, U., Kärcher, B., Ponater, M., Gierens, K., and Gettelman, A.: Contrail cirrus supporting areas in model and observations, Geophysical Research Letters, 35, https://doi.org/10.1029/2008GL034056, 2008.

Castino, F., Yin, F., Grewe, V., Yamashita, H., Matthes, S., Dietmüller, S., Baumann, S., Soler, M., Simorgh, A., Mendiguchia Meuser, M., Linke, F., and Lührs, B.: Decision-making strategies implemented in SolFinder 1.0 to identify eco-efficient aircraft trajectories: Application study in AirTraf 3.0, Geoscientific Model Development, 17, 4031 – 4052, https://doi.org/10.5194/gmd-17-4031-2024, cited by: 0; All Open Access, Gold Open Access, Green Open Access, 2024.

Dahlmann, K., Grewe, V., Froemming, C., and Burkhardt, U.: Can we reliably assess climate mitigation options for air traffic scenarios despite large uncertainties in atmospheric processes?, Transportation Research Part D - Transport and Environment, 46, 40–55, https://doi.org/10.1016/j.trd.2016.03.006, 2016.

Dahlmann, K., Matthes, S., and Grewe, V.: Conversion of climate metrics for policy applications, Climate Policy, submitted, 2025.

Dee, D. P., Uppala, S. M., Simmons, A. J., Berrisford, P., Poli, P., Kobayashi, S., Andrae, U., Balmaseda, M. A., Balsamo, G., Bauer, P., Bechtold, P., Beljaars, A. C. M., van de Berg, L., Bidlot, J., Bormann, N., Delsol, C., Dragani, R., Fuentes, M., Geer, A. J., Haimberger, L., Healy, S. B., Hersbach, H., Hólm, E. V., Isaksen, L., Kållberg, P., Köhler, M., Matricardi, M., Mcnally, A. P., Monge-Sanz, B. M., Morcrette, J. ., Park, B. ., Peubey, C., de Rosnay, P., Tavolato, C., Thépaut, J. ., and Vitart, F.: The ERA-Interim reanalysis: Configuration and performance of the data assimilation system, Quarterly Journal of the Royal Meteorological Society, 137, 553–597, https://doi.org/10.1002/qj.828, 2011, 2011.

Dietmüller, S., Jöckel, P., Tost, H., Kunze, M., Gellhorn, C., Brinkop, S., Frömming, C., Ponater, M., Steil, B., Lauer, A., and Hendricks, J.: A new radiation infrastructure for the Modular Earth Submodel System (MESSy, based on version 2.51), Geoscientific Model Development, 9, 2209 – 2222, https://doi.org/10.5194/gmd-9-2209-2016, 2016.

Dietmüller, S., Matthes, S., Dahlmann, K., Yamashita, H., Simorgh, A., Soler, M., Linke, F., Lührs, B., Meuser, M. M., Weder, C., Grewe, V., Yin, F., and Castino, F.: A Python library for computing individual and merged non-CO2 algorithmic climate change functions: CLIMaCCF V1.0, Geoscientific Model Development, 16, 4405 – 4425, https://doi.org/10.5194/gmd-16-4405-2023, 2023.

Fichter, C.: Climate impact of air traffic emissions in dependency of the emission location and altitude, Ph.D. thesis, DLR-Forschungsbericht 2009-22, Cologne, Germany, (ISSN 1434-8454), 2009.

Frömming, C., Ponater, M., Burkhardt, U., Stenke, A., Pechtl, S., and Sausen, R.: Sensitivity of contrail coverage and contrail radiative forcing to selected key parameters, ATMOSPHERIC ENVIRONMENT, 45, 1483–1490, https://doi.org/10.1016/j.atmosenv.2010.11.033, 2011.

https://doi.org/10.5194/jecats-2026-7
Preprint. Discussion started: 5 May 2026

Frömming, C., Ponater, M., Dahlmann, K., Grewe, V., Lee, D., and Sausen, R.: Aviation-induced radiative forcing and surface temperature change in dependency of the emission altitude, JOURNAL OF GEOPHYSICAL RESEARCH-ATMOSPHERES, 117, https://doi.org/10.1029/2012JD018204, 2012.

Frömming, C., Grewe, V., Brinkop, S., Jöckel, P., Haslerud, A. S., Rosanka, S., Van Manen, J., and Matthes, S.: Influence of weather situation on non-CO2 aviation climate effects: The REACT4C climate change functions, Atmospheric Chemistry and Physics, 21, 9151 – 9172, https://doi.org/10.5194/acp-21-9151-2021, 2021.

Gauss, M., Isaksen, I. S. A., Lee, D. S., and Sovde, O. A.: Impact of aircraft NO_x emissions on the atmosphere -: tradeoffs to reduce the impact, ATMOSPHERIC CHEMISTRY AND PHYSICS, 6, 1529–1548, https://doi.org/10.5194/acp-6-1529-2006, 2006.

Gierens, K. and Vazquez-Navarro, M.: Statistical analysis of contrail lifetimes from a satellite perspective, Meteorologische Zeitschrift, 27, 183–193, https://doi.org/10.1127/metz/2018/0888, 2018.

Grewe, V. and Stenke, A.: AirClim: an efficient tool for climate evaluation of aircraft technology, Atmospheric Chemistry and Physics, 8, 4621–4639, https://doi.org/10.5194/acp-8-4621-2008, 2008.

Grewe, V., Dameris, M., Fichter, C., and Lee, D.: Impact of aircraft NO_x emissions.: Part 2:: Effects of lowering the flight altitude, METEOROLOGISCHE ZEITSCHRIFT, 11, 197–205, https://doi.org/10.1127/0941-2948/2002/0011-0197, 2002.

Grewe, V., Champougny, T., Matthes, S., Froemming, C., Brinkop, S., Sovde, O. A., Irvine, E. A., and Halscheidt, L.: Reduction of the air traffic's contribution to climate change: A REACT4C case study, Atmospheric Environment, 94, 616–625, https://doi.org/10.1016/j.atmosenv.2014.05.059, 2014.

Grewe, V., Frömming, C., Matthes, S., Brinkop, S., Ponater, M., Dietmüller, S., Jöckel, P., Garny, H., Tsati, E., Dahlmann, K., Søvde, O. A., Fuglestvedt, J., Berntsen, T. K., Shine, K. P., Irvine, E. A., Champougny, T., and Hullah, P.: Aircraft routing with minimal climate impact: the REACT4C climate cost function modelling approach (V1.0), Geoscientific Model Development, 7, 175–201, https://doi.org/10.5194/gmd-7-175-2014, 2014a.

Grewe, V., Dahlmann, K., Flink, J., Frömming, C., Ghosh, R., Gierens, K., Heller, R., Hendricks, J., Jöckel, P., Kaufmann, S., Kölker, K., Linke, F., Luchkova, T., Lührs, B., van Manen, J., Matthes, S., Minikin, A., Niklaß, M., Plohr, M., Righi, M., Rosanka, S., Schmitt, A., Schumann, U., Terekhov, I., Unterstrasser, S., Vazquez-Navarro, M., Voigt, C., Wicke, K., Yamashita, H., Zahn, A., and Ziereis, H.: Mitigating the climate impact from aviation: Achievements and results of the DLR WeCare project, Aerospace, 4, 34, https://doi.org/10.3390/aerospace4030034, 2017.

Hansen, J., Sato, M., and Ruedy, R.: Radiative forcing and climate response, Journal of Geophysical Research Atmospheres, 102, 6831 – 6864, https://doi.org/10.1029/96JD03436, 1997.

Hersbach, H., Bell, B., Berrisford, P., Hirahara, S., Horányi, A., Muñoz-Sabater, J., Nicolas, J., Peubey, C., Radu, R., Schepers, D., Simmons, A., Soci, C., Abdalla, S., Abellan, X., Balsamo, G., Bechtold, P., Biavati, G., Bidlot, J., Bonavita, M., De Chiara, G., Dahlgren, P., Dee, D., Diamantakis, M., Dragani, R., Flemming, J., Forbes, R., Fuentes, M., Geer, A., Haimberger, L., Healy, S., Hogan, R. J., Hólm, E., Janisková, M., Keeley, S., Laloyaux, P., Lopez, P., Lupu, C., Radnoti, G., de Rosnay, P., Rozum, I., Vamborg, F., Villaume, S., and Thépaut, J.-N.: The ERA5 global reanalysis, Quarterly Journal of the Royal Meteorological Society, 146, 1999 – 2049, https://doi.org/10.1002/qj.3803, 2020.

Hofer, S. M. and Gierens, K. M.: Kinematic properties of regions that can involve persistent contrails over the North Atlantic and Europe during April and May 2024, Atmospheric Chemistry and Physics, 25, 6843 – 6856, https://doi.org/10.5194/acp-25-6843-2025, 2025.

Houweling, S., Dentener, F., and Lelieveld, J.: The impact of nonmethane hydrocarbon compounds on tropospheric photochemistry, Journal of Geophysical Research: Atmospheres, 103, 10 673 – 10 696, https://doi.org/10.1029/97jd03582, 1998.

https://doi.org/10.5194/jecats-2026-7
Preprint. Discussion started: 5 May 2026

IPCC: Contribution of Working Group I to the Sixth Assessment Report of the Intergovernmental Panel on Climate Change, in: Climate Change 2021: The Physical Science Basis, edited by Masson-Delmotte, V., Zhai, P., Pirani, A., Connors, S., Péan, C., Berger, S., Caud, N., Chen, Y., Goldfarb, L., Gomis, M., Huang, M., Leitzell, K., Lonnoy, E., Matthews, J., Maycock, T., Waterfield, T., Yelekçi, O., Yu, R., and Zhou, B., Cambridge University Press, Cambridge, United Kingdom and New York, NY, USA, 2021.

Irvine, E. A., Hoskins, B. J., Shine, K. P., Lunnon, R. W., and Froemming, C.: Characterizing North Atlantic weather patterns for climate-optimal aircraft routing, Meteorological Applications, 20, 80–93, 2013.

Joeckel, P., Kerkweg, A., Pozzer, A., Sander, R., Tost, H., Riede, H., Baumgaertner, A., Gromov, S., and Kern, B.: Development cycle 2 of the Modular Earth Submodel System (MESSy2), GEOSCIENTIFIC MODEL DEVELOPMENT, 3, 717–752, https://doi.org/10.5194/gmd-3-717-2010, 2010.

Joeckel, P., Tost, H., Pozzer, A., Kunze, M., Kirner, O., Brenninkmeijer, C. A. M., Brinkop, S., Cai, D. S., Dyroff, C., Eckstein, J., Frank, F., Garny, H., Gottschaldt, K.-D., Graf, P., Grewe, V., Kerkweg, A., Kern, B., Matthes, S., Mertens, M., Meul, S., Neumaier, M., Nuetzel, M., Oberlaender-Hayn, S., Ruhnke, R., Runde, T., Sander, R., Scharffe, D., and Zahn, A.: Earth System Chemistry integrated Modelling (ESCiMo) with the Modular Earth Submodel System (MESSy) version 2.51, GEOSCIENTIFIC MODEL DEVELOPMENT, 9, 1153–1200, https://doi.org/10.5194/gmd-9-1153-2016, 2016.

Kärcher, B., Burkhardt, U., Ponater, M., and Frömming, C.: Importance of representing optical depth variability for estimates of global line-shaped contrail radiative forcing, Proceedings of the National Academy of Sciences of the United States of America, 107, 19 181 – 19 184, https://doi.org/10.1073/pnas.1005555107, 2010.

Klingaman, E. and Shine, K. P.: Contrail algorithmic Climate Change Function derivation, supplement of Yin et al., Predicting the climate impact of aviation for en-route emissions: The algorithmic climate change function submodel ACCF 1.0 of EMAC 2.53, GEOSCIENTIFIC MODEL DEVELOPMENT, 16, 3313–3334, https://doi.org/10.5194/gmd-16-3313-2023, 2023.

Lee, D., Fahey, D., Skowron, A., Allen, M., Burkhardt, U., Chen, Q., Doherty, S., Freeman, S., Forster, P., Fuglestvedt, J., Gettelman, A., De León, R., Lim, L., Lund, M., Millar, R., Owen, B., Penner, J., Pitari, G., Prather, M., Sausen, R., and Wilcox, L.: The contribution of global aviation to anthropogenic climate forcing for 2000 to 2018, Atmospheric Environment, 244, https://doi.org/10.1016/j.atmosenv.2020.117834, 2021.

Lührs, B., Linke, F., Matthes, S., Grewe, V., and Yin, F.: Climate impact mitigation potential of European air traffic in a weather situation with strong contrail formation, Aerospace, 8, 1 – 15, https://doi.org/10.3390/aerospace8020050, 2021.

Markowicz, K. M. and Witek, M. L.: Simulations of Contrail Optical Properties and Radiative Forcing for Various Crystal Shapes, Journal of Applied Meteorology and Climatology, 50, 1740–1755, https://doi.org/10.1175/2011JAMC2618.1, 2011.

Marquart, S., Ponater, M., Mager, F., and Sausen, R.: Future development of contrail cover, optical depth, and radiative forcing: Impacts of increasing air traffic and climate change, Journal of Climate, 16, 2890 – 2904, https://doi.org/10.1175/1520-0442(2003)016<2890:FDOCCO>2.0.CO;2, 2003.

Matthes, S., Schumann, U., Grewe, V., Frömming, C., Dahlmann, K., Koch, A., and Mannstein, H.: Climate optimized air transport, in: Atmospheric Physics: Background – Methods – Trends, edited by Schumann, U., p. 877, Springer, Berlin/Heidelberg, Germany, https://doi.org/10.1007/978-3-642-30183-4_44, 2012.

Matthes, S., Gierens, K., Beckmann, B., Bugliaro, L., Dietmüller, S., Frömming, C., Hanst, M., Hofer, S., Jene, J., Kirschler, S., Köhler, C. G., Lau, A., Leemüller, R., Liedtke, A., Mendiguchia Meuser, M., Peter, P., Santos Gabriel, V., Köhler, I., Saueressig, G., Schlemmer, L., Sperling, J., Schlobach, S., Schultz, R., and von Sack, K.and Waltenberg, N.: D-KULT: data and tools for routine eco-efficient flight operations, J. Env. Com. Air Transp. Sys. Discuss. [preprint], in review, https://doi.org/https://doi.org/10.5194/jecats-2026-3, 2026.

https://doi.org/10.5194/jecats-2026-7
Preprint. Discussion started: 5 May 2026

Meerkötter, R., Schumann, U., Doelling, D., Minnis, P., Nakajima, T., and Tsushima, Y.: Radiative forcing by contrails, Annales Geophysicae, 17, 1080 – 1094, https://doi.org/10.1007/s00585-999-1080-7, 1999.

Megill, L., Deck, K., and Grewe, V.: Alternative climate metrics to the Global Warming Potential are more suitable for assessing aviation non-CO2 effects, Communications Earth and Environment, 5, https://doi.org/10.1038/s43247-024-01423-6, 2024.

Methven, J.: Offline Trajectories: Calculation and Accuracy, Ph.D. thesis, Technical Report, Departement of Meteorology, University of Reading, Reading, U.K., 1997.

Niklaß, M., Lührs, B., Grewe, V., Dahlmann, K., Luchkova, T., Linke, F., and Gollnick, V.: Potential to reduce the climate impact of aviation by climate restricted airspaces, Transport Policy, 83, https://doi.org/10.1016/j.tranpol.2016.12.010, 2019.

Peter, P., Matthes, S., Frömming, C., Jöckel, P., Bugliaro, L., Giez, A., Krämer, M., and Grewe, V.: Influence of temperature and humidity on contrail formation regions in the general circulation model EMAC: a spring case study, Atmospheric Chemistry and Physics, 25, 5911 – 5934, https://doi.org/10.5194/acp-25-5911-2025, 2025.

Peter, P., Matthes, S., Frömming, C., Jöckel, P., Brinkop, S., and Grewe, V.: Model Developments of the EMAC Contrail Submodel and Their Implications for Contrail Climate Change Functions, manuscript in preparation for Geoscientific Model Development (GMD), 2026.

Rao, P., Dwight, R., Singh, D., Maruhashi, J., Dedoussi, I., Grewe, V., and Frömming, C.: The ozone radiative forcing of nitrogen oxide emissions from aviation can be estimated using a probabilistic approach, Communications Earth and Environment, 5, https://doi.org/10.1038/s43247-024-01691-2, 2024.

Rap, A., Forster, P. M., Jones, A., Boucher, O., Haywood, J. M., Bellouin, N., and De Leon, R. R.: Parameterization of contrails in the UK Met Office Climate Model, JOURNAL OF GEOPHYSICAL RESEARCH-ATMOSPHERES, 115, https://doi.org/10.1029/2009JD012443, 2010.

Reithmeier, C. and Sausen, R.: ATTILA: atmospheric tracer transport in a Lagrangian model, Tellus B, 54, 278–299, 2002.

Righi, M., Hendricks, J., and Brinkop, S.: The global impact of the transport sectors on the atmospheric aerosol and the resulting climate effects under the Shared Socioeconomic Pathways (SSPs), Earth System Dynamics, 14, 835 – 859, https://doi.org/10.5194/esd-14-835-2023, 2023.

Roeckner, E., Brokopf, R., Esch, M., Giorgetta, M. A., Hagemann, S., Kornblueh, L., Manzini, E., Schlese, U., and Schulzweida, U.: Sensitivity of simulated climate to horizontal and vertical resolution in the ECHAM5 atmosphere model, Journal of Climate, 19, 3771 – 3791, https://doi.org/10.1175/JCLI3824.1, 2006.

Rosanka, S., Frömming, C., and Grewe, V.: The impact of weather patterns and related transport processes on aviation's contribution to ozone and methane concentrations from NO_x emissions, Atmospheric Chemistry and Physics, 20, 12 347–12 361, https://doi.org/10.5194/acp-20-12347-2020, 2020.

Sander, R., Baumgaertner, A., Gromov, S., Harder, H., Jöckel, P., Kerkweg, A., Kubistin, D., Regelin, E., Riede, H., Sandu, A., Taraborrelli, D., Tost, H., and Xie, Z.-Q.: The atmospheric chemistry box model CAABA/MECCA-3.0, Geoscientific Model Development, 4, 373 – 380, https://doi.org/10.5194/gmd-4-373-2011, 2011.

Sanz-Morere, I., Eastham, S. D., Allroggen, F., Speth, R. L., and Barrett, S. R. H.: Impacts of multi-layer overlap on contrail radiative forcing, Atmospheric Chemistry and Physics, 21, 1649–1681, https://doi.org/10.5194/acp-21-1649-2021, 2021.

Schumann, U.: On conditions for contrail formation from aircraft exhausts, Meteorol. Z., 5, 4–23, 1996.

Schumann, U., Mayer, B., Graf, K., and Mannstein, H.: A parametric radiative forcing model for contrail cirrus, Journal of Applied Meteorology and Climatology, 51, 1391 – 1406, https://doi.org/10.1175/JAMC-D-11-0242.1, 2012.

https://doi.org/10.5194/jecats-2026-7
Preprint. Discussion started: 5 May 2026

Schumann, U., Penner, J. E., Chen, Y., Zhou, C., and Graf, K.: On dehydration effects from contrails in a coupled contrail-climate model, Atmospheric Chemistry and Physics, 2015, 11 179–11 199, https://doi.org/10.5194/acp-15-11179-201, 2015.

Simorgh, A. and Soler, M.: Climate-optimized flight planning can effectively reduce the environmental footprint of aviation in Europe at low operational costs, Communications Earth and Environment, 6, https://doi.org/10.1038/s43247-025-02031-8, 2025.

Simorgh, A., Soler, M., Dietmüller, S., Matthes, S., Yamashita, H., Castino, F., and Yin, F.: Robust 4D climate-optimal aircraft trajectory planning under weather-induced uncertainties: Free-routing airspace, Transportation Research Part D: Transport and Environment, 131, https://doi.org/10.1016/j.trd.2024.104196, 2024.

Sonabend-W, A., Elkin, C., Dean, T., Dudley, J., Ali, N., Blickstein, J., Brand, E., Broshears, B., Chen, S., Engberg, Z., Galyen, M., Geraedts, S., Goyal, N., Grenham, R., Hager, U., Hecker, D., Jany, M., McCloskey, K., Ng, J., Norris, B., Opel, F., Rothenberg, J., Sankar, T., Sanekommu, D., Sarna, A., Schütt, O., Shapiro, M., Soh, R., Van Arsdale, C., and Platt, J. C.: Feasibility test of per-flight contrail avoidance in commercial aviation, Communications Engineering, 3, https://doi.org/10.1038/s44172-024-00329-7, 2024.

Stuber, N.: Ursachen der Variabilität des Klimasensitivitätsparameters für räumlich inhomogene Ozonstörungen, Ph.D. thesis, DLR-Forschungsbericht 2003-03, Cologne, Germany, (ISSN 1434-8454), 2003.

Stuber, N., Sausen, R., and Ponater, M.: Stratosphere adjusted radiative forcing calculations in a comprehensive climate model, Theoretical and Applied Climatology, 68, 125 – 135, https://doi.org/10.1007/s007040170041, 2001.

Teoh, R., Schumann, U., Gryspeerdt, E., Shapiro, M., Molloy, J., Koudis, G., Voigt, C., and Stettler, M. E.: Aviation contrail climate effects in the North Atlantic from 2016 to 2021, Atmospheric Chemistry and Physics, 22, 10 919 – 10 935, https://www.scopus.com/inward/record.uri?eid=2-s2.0-85137808141&doi=10.5194%2facp-22-10919-2022&partnerID=40&md5=96cc78fd3caca60542dd8929d5c58c30, 2022.

van Manen, J. and Grewe, V.: Algorithmic climate change functions for the use in eco-efficient flight planning, Transportation Research Part D: Transport and Environment, 67, 388–405, 2019.

van't Hoff, J. A., Hauglustaine, D., Pletzer, J., Skowron, A., Grewe, V., Matthes, S., Meuser, M. M., Thor, R. N., and Dedoussi, I. C.: Multi-model assessment of the atmospheric and radiative effects of supersonic transport aircraft, Atmospheric Chemistry and Physics, 25, 2515 – 2550, https://doi.org/10.5194/acp-25-2515-2025, 2025.

Voigt, C., Schumann, U., Minikin, A., Abdelmonem, A., Afchine, A., Borrmann, S., Boettcher, M., Bucuchholz, B., Bugliaro, L., Costa, A., Curtius, J., Dollner, M., Doernbrack, A., Dreiling, V., Ebert, V., Ehrlich, A., Fix, A., Forster, L., Frank, F., Fuetterer, D., Giez, A., Graf, K., Grooss, J.-U., Gross, S., Heimerl, K., Heinold, B., Hueneke, T., Jaervinen, E., Jurkat, T., Kaufmann, S., Kenntner, M., Klingebiel, M., Klimach, T., Kohl, R., Kraemer, M., Krisna, T. C., Luebke, A., Mayer, B., Mertes, S., Molleker, S., Petzold, A., Pfeilsticker, K., Port, M., Rapp, M., Reutter, P., Rolf, C., Rose, D., Sauer, D., Schaefer, A., Schlage, R., Schnaiter, M., Schneider, J., Spelten, N., Spichtinger, P., Stock, P., Walser, A., Weigel, R., Weinzierl, B., Wendisch, M., Werner, F., Wernli, H., Wirth, M., Zahn, A., Ziereis, H., and Zoger, M.: ML-CIRRUS – The airborne experiment on natural cirrus and contrail cirrus with the high-altitude long-range research aircraft HALO, Bulletin of the American Meteorological Society, 98, 271–288, https://doi.org/10.1175/BAMS-D-15-00213.1, 2017.

Yin, F., Grewe, V., Castino, F., Rao, P., Matthes, S., Dahlmann, K., Dietmüller, S., Frömming, C., Yamashita, H., Peter, P., et al.: Predicting the climate impact of aviation for en-route emissions: the algorithmic climate change function submodel ACCF 1.0 of EMAC 2.53, Geoscientific Model Development, 16, 3313–3334, 2023.